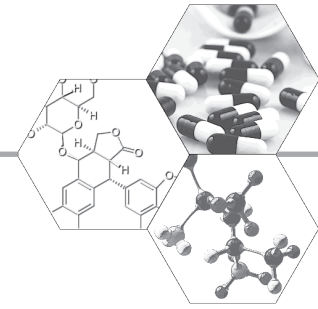



# Magnetic iron oxide nanoparticles for biomedical applications

Due to their high magnetization, superparamagnetic iron oxide nanoparticles induce an important decrease in the transverse relaxation of water protons and are, therefore, very efficient negative MRI contrast agents. The knowledge and control of the chemical and physical characteristics of nanoparticles are of great importance. The choice of the synthesis method (microemulsions, sol-gel synthesis, laser pyrolysis, sonochemical synthesis or coprecipitation) determines the magnetic nanoparticle's size and shape, as well as its size distribution and surface chemistry. Nanoparticles can be used for numerous *in vivo* applications, such as MRI contrast enhancement and hyperthermia drug delivery. New developments focus on targeting through molecular imaging and cell tracking.

Superparamagnetic iron oxide nanoparticles are widely used for biotechnology and medical applications, including contrast agents for MRI, cell recognition and separation and drug delivery [1,2]. Based on the iron oxide particles' surface and their size, which influence the biodistribution, some clinical applications have been developed: detection of liver tumors, metastatic lymph nodes, inflammatory and degenerative diseases. They are also suitable for functional MRI to display dysfunctional processes on the basis of cellular and molecular mechanisms [3].

Iron oxide nanoparticles can be divided into three categories: superparamagnetic iron oxide (SPIO), which present a hydrodynamic diameter larger than 50 nm, ultrasmall (U)SPIO, characterized by a hydrodynamic diameter less than 50 nm and micron-sized particles of iron oxide (MPIO). Subsets of USPIO are also known as very small particles of iron oxide (VSOP, 7–9 nm) and monocrystalline iron oxide nanoparticles (MION, 10–30 nm). They have a longer plasmatic half-life and exhibit slower uptake by liver and spleen after intravenous administration **(Table 1)**. SPIO are polycrystalline compounds with a hydrodynamic diameter between 60–180 nm. They are mainly used via intravenous infusion to detect and characterize small lesions in the liver or to visualize the digestive tract **(Table 2)**. Both described nanoparticles are most often formulated with dextran or dextran derivatives.

## Synthesis of iron oxide nanoparticles

### ■ Coprecipitation in aqueous medium

Magnetite can be obtained in various ways [1,4,5]. The first method consists of a partial reduction of aqueous ferric salt, followed by a precipitation in alkaline medium [6]. The second technique, introduced by Sugimoto and Matijevic [7], implies the oxidation of an aqueous ferrous salt solution by ion nitrates, allowing the formation of iron oxide nanoparticles with a diameter between 30–100 nm. However, most of the publications refer to the synthesis introduced by Massart [8]. This process allows a reproducible formation of spherical particles in great quantity and does not require expensive material. The method of synthesis is rather simple and is based on an alkaline coprecipitation of ferrous and ferric salt precursors in aqueous medium in a stoechiometric ratio $Fe^{2+}/Fe^{3+} = 0.5$ [9–11].

At room temperature, this coprecipitation forms quasi-instantaneously magnetite **(Figure 1A)**. The more frequent case is the formation of the maghemite by oxygen chemisorption on magnetite **(Figure 1B)**. To preserve the crystalline state of magnetite, it is possible to use a $Fe^{2+}/Fe^{3+}$ ratio higher than 0.5 or to work under an inert nitrogen atmosphere. This flushing prevents the oxidation of magnetite but can also cause a reduction of the size of particles [12]. Colloidal magnetite dispersions are then obtained after peptization by either $HNO_3$ or by $N(CH_3)_4OH$ **(Figure 1C)**.

This method of synthesis leads to quasi-spherical particles and has the advantage of being fast, simple, economic and easily transposable on a large scale; however, the particles obtained present a high index of polydispersity and a later procedure for selection of size is often required.

### ■ Reverse microemulsions

Another strategy consists of using microemulsions as nanoreactors to synthesize superparamagnetic nanoparticles. This process allows control of the

**Sophie Laurent, Jean-Luc Bridot, Luce Vander Elst & Robert N Muller†**
†Author for correspondence
Department of General, Organic and Biomedical Chemistry, NMR and Molecular Imaging Laboratory, University of Mons, B-7000 Mons, Belgium
Tel.: +3 265 373 520
Fax: +3 265 373 533
E-mail: robert.muller@umons.ac.be

**Superparamagnetism**
Form of magnetism, which appears in ferromagnetic or ferrimagnetic nanoparticles

**Hydrodynamic diameters**
Global size of the core with the coating

FUTURE SCIENCE part of fsg

**Table 1. Nonexhaustive list of ultrasmall superparamagnetic iron oxide contrast agents.**

| Short name/generic name/ trade name | Iron oxide core diameter (TEM)/ hydrodynamic diameter (PCS) (nm) | Relaxivity ($s^{-1}mM^{-1}$) | Applications | Ref. |
|---|---|---|---|---|
| AMI-227<br>Ferumoxtran<br>Sinerem®, Combidex®<br>Coating: dextran | 4–6<br>20–40 | $R_1$ = 19.5<br>$R_2$ = 87.6<br>(1.5 T) | Liver, spleen and lymph nodes<br>Blood-pool agent for MR angiography<br>*In vivo* MRI of macrophage activity in inflammatory areas<br>*In vitro* cellular magnetic labeling | [163–167] |
| SHU 555C<br>Ferucarbotran<br>Supravist®<br>Coating: carboxydextran | 3–4<br>30 (17–46) | $R_1$ = 10.7<br>$R_2$ = 38<br>(1.5 T) | Blood-pool agent for MR angiography<br>*In vivo* MRI of macrophage activity in inflammatory areas<br>*In vitro* cellular magnetic labeling | [164,167–170] |
| NC100150<br>Ferruglose PEG-feron<br>Clariscan®<br>Coating: carbohydrate polyethyleneglycol | 5–7<br>20 | $R_1$ = 20<br>$R_2$ = 35<br>(0.47 T) | Blood-pool agent for MR angiography and perfusion MRI | [164,165] |
| Ferumoxytol<br>Coating: semisynthetic carbohydrate (polyglucose sorbitol carboxymethyl ether) | 6.7 ± 0.4<br>30 ± 2 | $R_1$ = 15<br>$R_2$ = 89<br>(1.5 T) | Blood-pool agent for MR angiography<br>*In vivo* MRI of macrophage activity | [166,167, 171,301] |
| MION-46L<br>Coating: dextran | 4.6 ± 1.2<br>8–20 | $R_1$ = 3.95<br>$R_2$ = 19.6<br>(1.5 T) | Blood-pool agent<br>Receptor-targeted MRI and *in vivo* and *in vitro* magnetic cellular labeling | [171,178–183] |
| VSOP-C184<br>Coating: citrate | 4–5<br>7–9 | $R_1$ = 14<br>$R_2$ = 33.4<br>(1.5 T) | Liver<br>Blood-pool agent for MR angiography<br>*In vivo* MRI of macrophage activity in inflammatory areas | [164,178–182] |

*MION: Monocrystalline iron oxide nanoparticle; PCS: Photon correlation spectroscopy; TEM: Transmission electron microscopy.*

radius of the particles by exploiting the size of the reactors and the quantity of precursors available in each emulsion **(Figure 2)**. It differs by the use of anionic or cationic surfactants, such as sodium dioctylsulphosuccinate [13], cetyltrimethylammonium bromide [14], sodium dodecylsulphate [15] or neutral compounds including the polyethoxylates (Igepal, Brij or Tween) [16]. These surfactants allow control of the size of the particles by limiting the phenomena of crystalline growth and agglomeration of the nanoparticles.

Other parameters can also regulate the size, such as the concentration of metals, the nature and concentration of the base or the temperature [17,18]. In spite of obtaining particles of controlled size and distribution of narrow size, this technique requires large amounts of surfactant (up to 20–30%), which is difficult to eliminate and limited to the laboratory scale [19].

### ■ Hydrothermal methods

A third method for the formation of single-crystal iron oxide slightly polydisperse particles [20,21] is the hydrothermal decomposition of organometallic precursors, such as the iron acetylacetonate or iron carbonates, in the presence of a surfactant, such as a long carbon chain with carboxylic functions or amines. The hydrothermal reactions are aqueous reactions carried out under conditions in which the temperature and the pressure can go beyond 200°C and 14 bars, respectively. These conditions make it possible to largely modify the physicochemical properties of an aqueous solvent. Under these conditions, water is not only the solvent but also a reagent able to accelerate the reactions of hydrolysis. Various examples of thermal decomposition are described in the literature [22–25].

Thermal decomposition can also be carried out in an organic solvent. Sun *et al.* have synthesized MIONs by thermal decomposition of iron acetylacetonate(III) in the presence of oleic acid, oleylamine and 1,2-hexadecanediol in the high boiling solvents phenyl ether and benzyl ether [26]. A 'seeded-growth' procedure, which consists of adding to the reactional medium a given amount of small particles (radius of 2 nm), makes it possible to obtain larger particles with

**Table 2. Nonexhaustive list of superparamagnetic iron oxide and micron-sized particles of iron oxide contrast agents.**

| Short name/generic name/trade name | Iron oxide core diameter (TEM)/ hydrodynamic diameter (PCS) (nm) | Relaxivity ($s^{-1}mM^{-1}$) | Applications | Ref. |
|---|---|---|---|---|
| AMI-25<br>Ferumoxide<br>Endorem®, Feridex®<br>Coating: dextran | 4.8–5.6<br>80–150 | $R_1$ = 9.95<br>$R_2$ = 158<br>(1.5 T) | Liver, spleen and bone marrow<br>*In vitro* cellular magnetic labeling | [163–166, 169,172,173] |
| SHU 555A<br>Ferucarbotran<br>Resovist®<br>Coating: carboxydextran | 4.2 (3–5)<br>62 | $R_1$ = 9.7<br>$R_2$ = 189<br>(1.5 T) | Liver, spleen<br>MR angiography perfusion MRI<br>*In vitro* cellular magnetic labeling | [165,168, 169,175] |
| AMI-121<br>Ferumoxil<br>Lumirem®, Gastromark®<br>Coating: silicone | 300 | | Digestive tract | [183,184 |
| Ferristene<br>Abdoscan®<br>Coating: Styrene/divinyl benzene | 3500 | | Digestive tract | [165,185] |
| MION-liposomes<br>Coating: liposomes | 16 ± 4<br>170–360 | $R_1$ = 3<br>$R_2$ = 240<br>(1.5 T) | Liver, spleen and bone marrow<br>Drug delivery | [186] |

*MION: Monocrystalline iron oxide nanoparticle; PCS: Photon correlation spectroscopy; TEM: Transmission electron microscopy.*

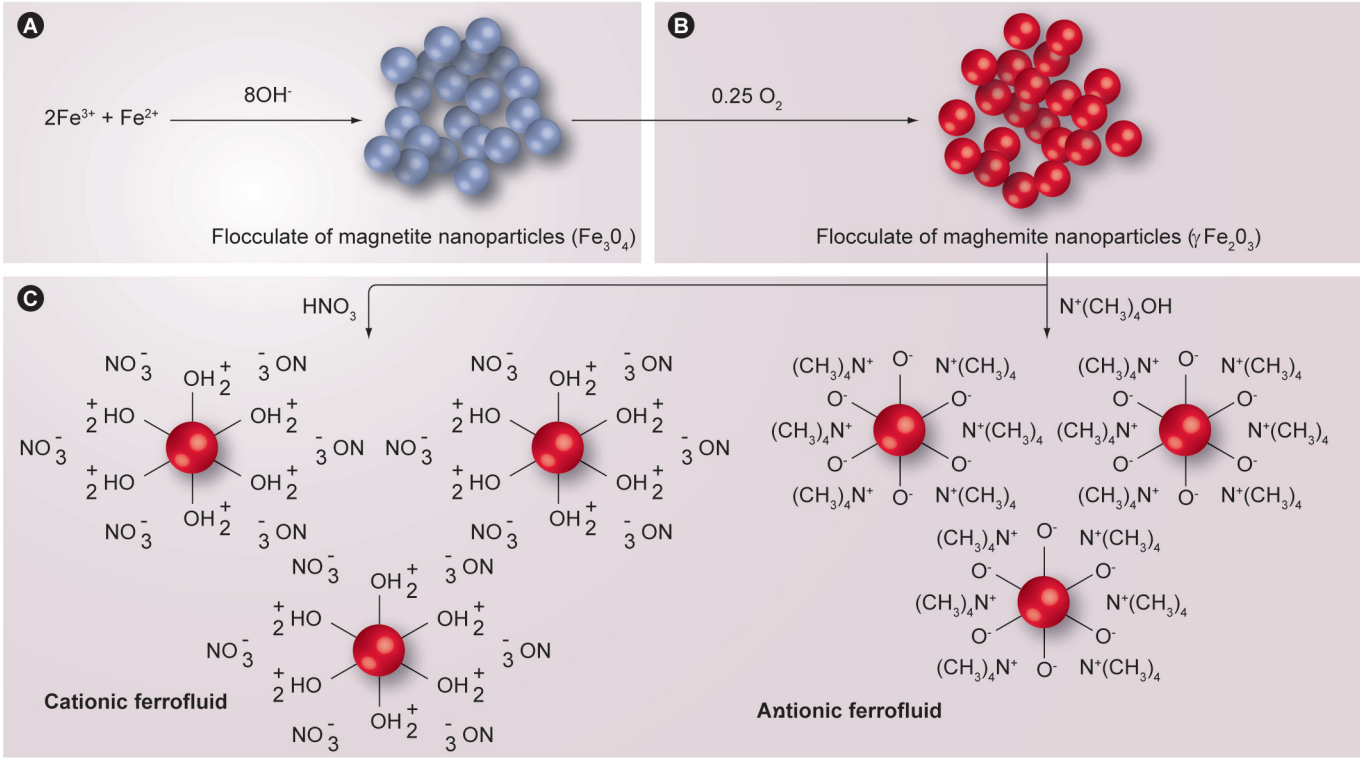


**Figure 1. Coprecipitation.**
Data from [8].

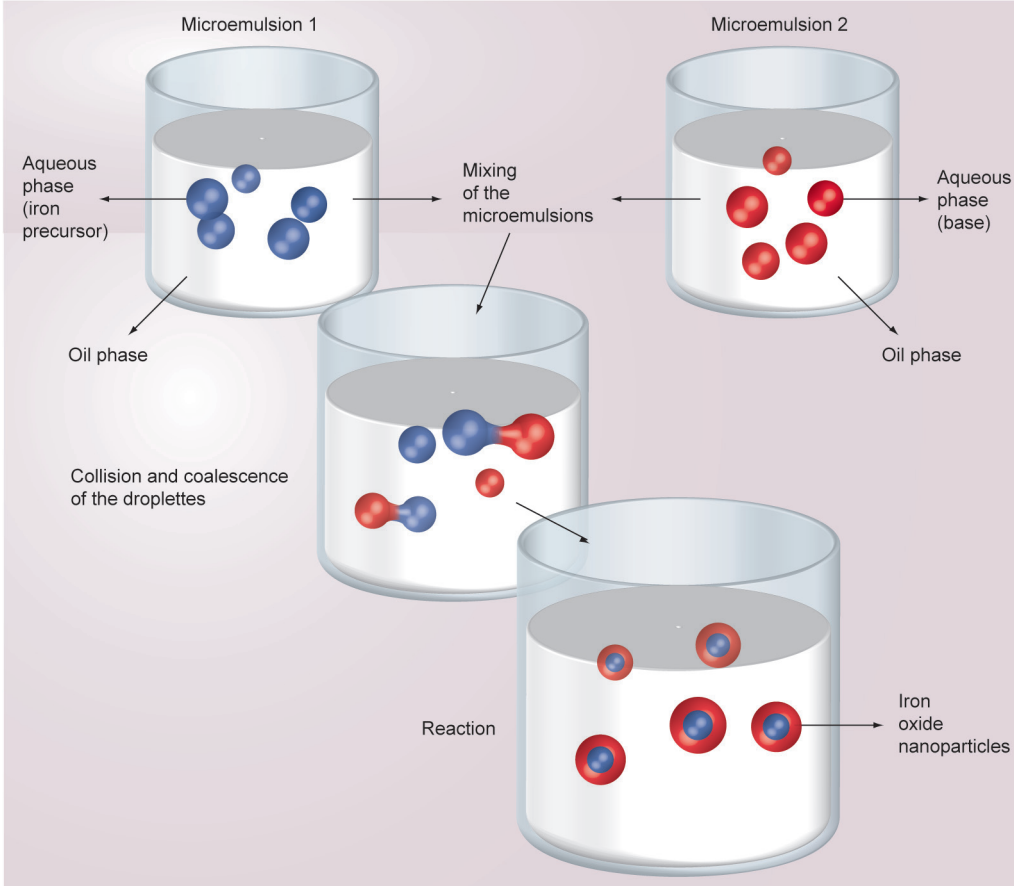


**Figure 2. Synthesis of nanoparticles by the microemulsion method.**

well-defined radii (up to 8 nm). These authors also proposed a relatively simple method to access hydrophilic nanoparticles by addition of a bipolar surfactant.

The crystals formed by hydrothermal treatment are generally nonaggregated due to the presence of stabilizing agents. They are also characterized by a distribution of narrow size, as well as purity and a very high density [27].

## ■ Sol-gel methods

This process could be an interesting alternative because it consists of modifying the precursors at low temperature, hence the term 'soft chemistry'. It is quoted frequently in the literature as the method used to prepare ultrafine superparamagnetic powders [28].

The chemistry of this process brings into play successive hydrolysis and condensation reactions of inorganic species. The first of these, during which a water molecule gives rise to a reactive group (M-OH) by releasing an alcohol molecule, corresponds to the first step of the process. The formation of nanoparticles can take place by polycondensation (oxolation) and/or polyaddition (olation) reactions. During these, a reactive hydroxo group forms an oxo or hydroxo bridge by eliminating water or alcohol:

$$\text{M-OR} + \text{H}_2\text{O} \longrightarrow \text{M-OH} + \text{ROH}$$

**HYDROLYSIS REACTION**

$$\text{M-OH} + \text{M-OR} \longrightarrow \text{M-O-M} + \text{ROH}$$

**OXOLATION REACTION**

$$\text{M-OH} + \text{M-OH} \longrightarrow \text{M-O-M} + \text{H}_2\text{O}$$

**OLATION REACTION**

Slow and controlled speeds of hydrolysis generally lead to the formation of small particles [29]. The factors most likely to influence the kinetics of hydrolysis and condensation are the type of solvent, temperature, nature and concentration of the precursors or the pH [30]. This process of ground-freezing is also an adequate method to

synthesize nanoparticles coated in a matrix with silica [31–33]. Various studies have been based on the Stöber process, in which silica is directly deposited '*in situ*' on the nanoparticles through a step of hydrolysis and condensation of commercial precursors like tetraethoxysilane in a water/ethanol mixture [34]. This process makes it possible to control the thickness of the silica layer on the surface of the iron oxide nanoparticles. The ground-freezing technique nonetheless requires adapting the reactivity of the precursors by modifying their chemistry, a step that it is sometimes difficult to control.

### ■ Polyol methods

Initially dedicated to the synthesis of metal particles, due to the reducing character of polyols [35], this method was later adapted to synthesize highly crystalline magnetite nanoparticles [36], with a precise size and characteristic narrow-size distribution.

Caruntu *et al.* describe a mechanism that makes it possible to explain the formation of magnetite nanoparticles by hydrolysis of a ferrous-ferric mixture in alkaline medium and in the presence of diethylene glycol [37]. This mechanism comprises three main steps: metal complexation by a molecule of solvent, reactions of hydrolysis-condensation leading to a partially hydrated form and, finally, the dehydration of the nanoparticles [38].

The use of polyols in this method is flexible and presents various advantages. Indeed, because of their important permittivity, high boiling point and the ability to use them for complexation, polyols simultaneously play a role not only as a solvent and reducing agent, but also as a surfactant, by limiting the phenomena of agglomeration [39]. The presence of these glycol groups absorbed on the nanoparticle's surface on the one hand slows down the oxidation of magnetite but, on the other, allows easy dispersion in polar solvents such as water. A last advantage of this process is the absence of additional reducing agent and of surfactant in the reactional medium, making this process adaptable on a large scale.

### ■ Sonochemistry methods

Decomposition of the iron precursors by sonochemistry can also lead to the formation of iron-oxide nanoparticles [40,41]. This process is based on the passage of high frequency sound waves (20 KHz to 10 MHz) through a solution containing the organometallic precursors giving place to the formation, growth and implosion of bubbles in the liquid at room temperature [42]. The powders formed by sonochemistry are generally amorphous, porous and agglomerated [43]. The fast bursting of bubbles also limits the mechanism of crystalline growth of the nucleons, so the nanoparticles are generally of a small size.

Surfactants (e.g., OTS and oleic acid) or polymers (e.g., polyvinyl alcohol solution and chitosan) can also be added during or after the stage of sonication to ensure the formation of a stable dispersion of nanoparticles [44,45]. The main advantages of this technique are the use of few reagents and the requirement of less purification steps [46]. However, a very particular experimental device is required.

### ■ Pyrolytic methods

Although not very economic, physical pyrolytic methods are being increasingly used as they allow the fast formation of uniform magnetic particles, according to experimental parameters, such as the nature of the precursors, the reagent flow rate in the pyrolysis zone or the laser power [47–50]. The advantage of this type of protocol is its great flexibility, which makes it possible to widely vary the product's chemical composition, size and crystallinity. This method was also adapted for the preparation of nanoparticles of maghemite, stabilized by a silicon coating [51]. The main constraints of this method are related to the need for a specific reagent/laser resonance and to the requirement of a specific installation.

## Stabilization

According to the application intended for these ferrofluids, several types of steric or electrostatic protections can be used. In the biomedical field, the biocompatibility and biodeterioration will control the choice of stabilizing matrix.

These stabilizing agents, steric or electrostatic, are mainly made up of inorganic materials, natural surfactants or synthetic polymeric matrices. The challenge is to create a sufficiently strong repelling power between the nanoparticles and decrease the interfacial tension of the system, in order to obtain stable ferrofluids [52]. During coprecipitation, the iron oxide particles are characterized by high surface/volume ratio, due to the small size of the obtained nanoparticles and the system spontaneously tends to minimize the interfacial tension by causing their agglomeration. Since this

interfacial tension depends primarily on the phenomena of adsorption and, consequently, on the chemical composition of the interface, one can expect that the addition of agents can also control the thermodynamic stability of these iron oxide colloids.

### ■ Steric stabilization: natural or synthetic polymeric matrices

Two approaches are normally used to allow the stabilization of ferrofluids in the presence of polymers. In the first approach, nanoparticles are directly formed in the presence of a polymeric matrix. This matrix, used as a nanoreactor, can control at the same time the size and the monodispersity of the nanoparticles. Among the many examples described in the literature, Hu *et al.* based their work on the precipitation of iron precursors in an aqueous polyvinyl alcohol solution, a porous polymer structure [53]. The second approach consists of grafting polymers onto the surface of the magnetite nanoparticles after their formation. Electrosteric stabilization occurs when the polymers are charged. Some of these natural or synthetic polymers are listed in **Table 3** [54–62].

The natural polymer usually used to improve stabilization of the nanoparticles is dextran, thanks to its biocompatibility and biodeterioration [63]. Molday and Mackenzie were the first to describe the formation of magnetite in the presence of dextran 40000 [64]. At the present time, the commercial contrast agents are generally made up of iron oxide nanoparticles coated with dextran [65], or with its derivatives, such as carboxydextran [66] (Ferucarbotran® and Resovist®) or carboxymethyldextran (Ferumoxytol®) [67].

The mechanism of adsorption of the dextran on the surface of the iron oxide nanoparticles results primarily from hydrogen bonds between the polar functional groups distributed on the chain of the polymer and the hydroxylated and proton sites at the particles' surface. The length of the dextran chain represents an important choice for nanoparticle stabilization. This mechanism of nonspecific adsorption can also be observed for other neutral macromolecules, such as ethylene polyoxide or polyacrylamide in aqueous solution. The polyelectrolytes, such as the alginate [68] or ionic surfactants, are more strongly adsorbed on these charged magnetic surfaces. Indeed, the energy of adsorption includes, in addition to a steric repulsion, an electrostatic contribution due to the interactions between sites of opposed charge on surface and polymer. In addition to the dextran, other natural polymers such as chitosan [69], gelatin [70], or pullulan [71] can allow obtaining magnetic ferrofluids.

Among synthetic polymers, PEG is often used, mainly thanks to its properties of hydrophilicity and biocompatibility. Indeed, the presence of PEG molecules on the surface of the nanoparticles not only improves their steric stabilization but also makes it possible to prolong the plasmatic half-life *in vivo* [72]. Recently, Kumagai *et al.* presented a new method for stabilization of the iron oxide nanoparticles by using a copolymer of PEG – poly(acid aspartic) [73]. These PEG-PAsp molecules are coordinated to the surface of the iron oxide nanoparticles by the carboxylic acids of the polyaspartic acid and the surface of the iron oxide nanoparticles. Other copolymers can also participate in the formation of stable ferrofluids; including poly(lactide-Co-glycolide), mainly used for its biocompatibility and its biodeterioration and which, moreover, is approved by the US FDA for pharmaceutical use in drug delivery [73].

Poly(ethyleneimine) also participates in the formation of stable ferrofluids at a broad range of pHs [74]. Moreover, by forming cationic complexes, it can interact in a nonspecific way with negatively charged species, such as DNA or be internalized by endocytosis.

Recently, polymers or copolymers of an acrylic structure, such as polyacrylic acid [75] or polymethacrylic acid [76], are being used due to their capacity to increase stability and biocompatibility, as well as particle bioadhesion thanks to the carboxylate functions [77].

Other polymers found in the literature are polyvinylpyrrolidone [78], poly(lactic acid) [79], ethylcellulose [80], poly(ε-caprolactone) [81], arabinogalactane [82], polystyrene [83] and polyaniline [84].

Polyelectrolytes such as alginate [85,86] or ionic surfactants more strongly adsorb on these magnetic surfaces by a mechanism of chemisorption via the carboxylate functions. However, owing to the hydrophobic nature of the hydrocarbon chains of fatty acids, the nanoparticles are often dispersed in nonpolar solvents, which constitute an obstacle for any biological application. Khalafalla *et al.* demonstrated further that only the fatty acids of C10–C15 alkyl chains are able to form a structure of monolayer with a hydrophilic surface

**Table 3. Nonexhaustive list of polymeric coatings used to ensure steric stabilization of the superparamagnetic particles.**

| Polymer matrix | Characteristic of the polymer |
|---|---|
| ***Natural polymeric matrices*** | |
| Dextran | Biodegradable and biocompatible polymer<br>Can increase plasma half-life<br>Possibility of agglomeration during synthesis<br>Possibility of desorption by heating effect or dilution |
| Chitosan | Hydrophilic cationic, linear, biocompatible polymer<br>Presence of charges, better internalization compared with MRI Resovist®<br>Useful for drug delivery<br>Possibility of agglomeration during synthesis |
| Pullulan | Polysaccharide neutral, highly soluble in water, nontoxic<br>Targeting hepatocytes → particle accumulation in the liver |
| ***Synthetic polymer matrices*** | |
| PEG | Hydrophilic polymer, nonantigen<br>Prolongs plasma half-life by reducing cellular uptake |
| PVA | Hydrophilic and biocompatible polymer<br>Obtaining nonagglomerated and monodisperse particles<br>Formation of magnetic gels<br>Size control (nanoreactor) |
| PEI | Hydrophilic positively charged polymer, capable of interactions with nucleotides set for transfection applications and magnetic separation<br>Formation of stable ferrofluids on a wide range of pH |
| PLGA | Biocompatible and biodegradable, approved by the US FDA<br>Therapeutic use → drug delivery<br>Laborious process of coating and expensive<br>Low magnetization saturation values |
| Polyacrylic acid (e.g., PAA, PMMA and polyalkylcyanoacrylate) | Increased stability and biocompatibility of the particles<br>Help with bioadhesion |
| Alginate | Polysaccharide electrolyte → steric and electrostatic stabilization<br>Nanoreactor → size control<br>Biological applications → drug delivery |
| Diblock copolymers neutral/polyelectrolytes, PEOPMAA, PAA-chitosan, PSPA,PAN-PAM, PEG-PASP, | Steric and electrostatic stabilization<br>Offering a choice in the nature blocks and therefore tunable according to biological applications<br>Biocompatibility |

*PAA: Polyacrylic acid; PEG: Polyethylene glycol; PEI: Poly(ethyleneimine); PEO: poly(ethylene oxide); PLGA: Poly(lactide-Co-glycolide); PMMA: Poly(methyl methacrylate); PSPA: Polystyrenylphosphonous acid; PVA: Polyvinyl alcohol solution.*

and, consequently, make it possible to form a stable aqueous dispersion [87]. For others, a modification of their surface is necessary in order to transfer and disperse them in aqueous medium. Amphiphilic polymers, such as α-cyclodextrin [88], copolymers of the pluronic acid F127 [89] or chitosan [90] can be used to allow this dispersion in aqueous medium.

### ■ Electrostatic stabilization

Functional groups (e.g., carboxylate, sulphonate and sulphate) are able to adsorb on the nanoparticle surface **(TABLE 4)**. Their specific adsorption, by substitution of hydroxo ligands present on the surface of the iron oxide, causes important changes at the level of the interfacial properties. The modification of their isoelectric point improves their field of colloidal stability, in particular at a physiological pH. For example, citric acid [91], intervening during the formation of VSOP C184 [92], modifies the isoelectric point of magnetite at pH = 3 while coordinating with the three carboxylate functions on its surface **(FIGURE 3A)**. The biocompatibility of the phosphonate [93] or phosphate ligands may also be worth exploiting in order to obtain a colloidal dispersion that is stable and usable in various biological applications **(FIGURE 3B)**. Different studies [94] have shown the superiority of grafting the biphosphonate groups at physiological pH, allowing a level of grafting that is higher than that of the other

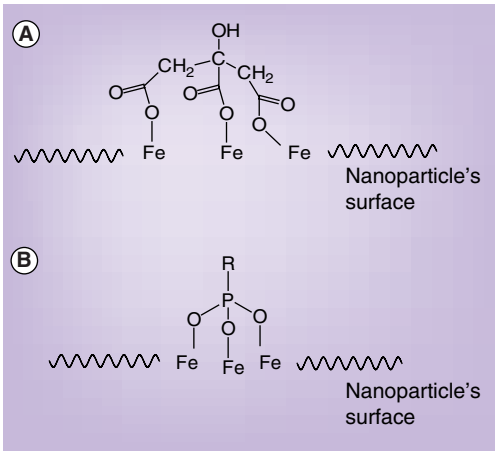


**Figure 3. (A) Citrate and (B) phosphonate derivatives on the iron oxide nanoparticle surface.**

functions of the carboxylate, sulphate or sulphonate types, mainly owing to the strong P-O-Fe bonds.

This type of stabilization remains, however, a noncovalent process of coordination between the particle's surface and the functional group and can pose problems for *in vivo* applications. One of the strategies to improve this mechanism of stabilization is to increase the number of anchoring points on the surface of the iron oxide nanoparticles. Roux *et al.* used this strategy to stabilize gold nanoparticles by using dihydrolipoic acid to improve colloidal stability of the nanoparticles via better adhesion on their surface [95].

Certain inorganic coatings, such as gold [96], alumina [97] or silica [98] also allow improvement of the stability in aqueous dispersion, as well as fictionalization of the magnetic particles for various biomedical applications. By ensuring simultaneously chemical stabilization on a broad pH range and biocompatibility, silica represents an ideal choice for obtaining stable ferrofluids [99,100].

This negatively charged silica coating allows a Coulomb repulsion between the magnetic nanoparticles [101]. Depending on the thickness of the silica layer, it is also possible to increase the shielding of the magnetic dipolar interactions between the iron-oxide particles. The last advantage of a surface enriched in silica is the presence of many silanol groups able to facilitate the processes of coupling on their surface, in particular with silanic coupling agents [102].

There are, in the literature, three approaches to generate magnetic nanoparticles covered with silica. The first method is the sol-gel process [103], in which the growth of the silica layer is carried out *in situ* through the hydrolysis and condensation of a precursor such as tetraethoxysilane on the magnetite surface.

The pyrolytic method leads most often to the formation of colloidal particles characterized by a broad distribution of size, contrary to the last method, based on an inverse microemulsion technique. The micelles are used to control the silica coating, allowing the formation of small size and monodisperse nanoparticles.

Among all the steric or electrostatic matrices most studied in recent years, the fictionalization of the iron oxide nanoparticles by silica and organosilane agents has aroused a particular interest. Silica has, indeed, many advantages: it allows a covalent stabilization on a broad range of pH, it is chemically inert, and it is cheap. The processes of coupling on its

**Table 4. Electrostatic coatings.**

| Nature of the coating | Main characteristics | Ref. |
|---|---|---|
| ***Nonpolymeric matrices*** | | |
| Functional groups (e.g., phosphate, carboxylate, sulphonate and [bi]phosphonate tartaric, gluconic or dimercaptosuccinic acid, phosphorylcholine and taurine). | Electrostatic stabilization of the nanoparticles by a mechanism of adsorption or coordination<br>Method sensitive to the pH | [187] |
| ***Inorganic matrices*** | | |
| Silica | Biocompatible and inert<br>Easy coupling process<br>Stabilization on a broad range of pH<br>Many prospects for various biological applications | [188] |
| Gold | The Fe/Au structure presents adequate surface for a later fictionalization<br>Various possible applications: among them drug delivery | [189] |

surface, in particular with the organosilanes, are simple. The interest in the use of silanic organofunctional agents ($R_nSiX_{(4-n)}$) is the relatively important diversity of their functional group R **(FIGURE 4)**, which offers the possibility of functionalizing the particles and, thus, of modulating their surface according to the biological criteria selected.

## ■ Evaluation of the colloidal stability

Characterization of size distribution and colloidal stability of iron oxide nanoparticles is very important in order to understand their implication on the biological application. The efficiency of the stabilization strategies can be estimated by different physical methods.

Among these techniques, photon correlation spectroscopy (PCS) or dynamic light scattering is based on the diffusion of a light beam by material in suspension. When the particle diameter is smaller than the wavelength of the incident light, in Rayleigh conditions, an isotropic scattering is observed by each particle, resulting in a global light intensity made of constructive and destructive contribution from each particles. In the case of a stable laser source, a fluctuation of the intensity of scattered light is observed over time and comes from the movement of particles in solution. This fluctuation may be analyzed by an autocorrelation function, which is the convolution of the fluctuation curve shifted by a time (τ) and allows the determination of the size distribution of the diffusing objects. The exponential function obtained is characterized by a time (T) that permits the determination of the diffusion coefficient of the particles and, subsequently, their size.

When diffusing objects in solution are assumed to be spherical, their hydrodynamic diameter determined by PCS can have different representation: intensity, volume and number [104].

Intensity representation mode corresponds to direct determination, with the τ volume and number representations, of the size after rescaling by the Mie theory. Volume size distributions are preferred for comparing results obtained with a mass distribution metrological technique and number for microscopy analysis. The formation of aggregated particles can be defined by an object characterized by a slower Brownian motion. It results in lower diffusion coefficient, which induces a higher hydrodynamic diameter than nonaggregate nanoparticles. Thus, an increase of the hydrodynamic size over time indicates an agglomeration of the particles, suggesting that the coating must be optimized for biological application.

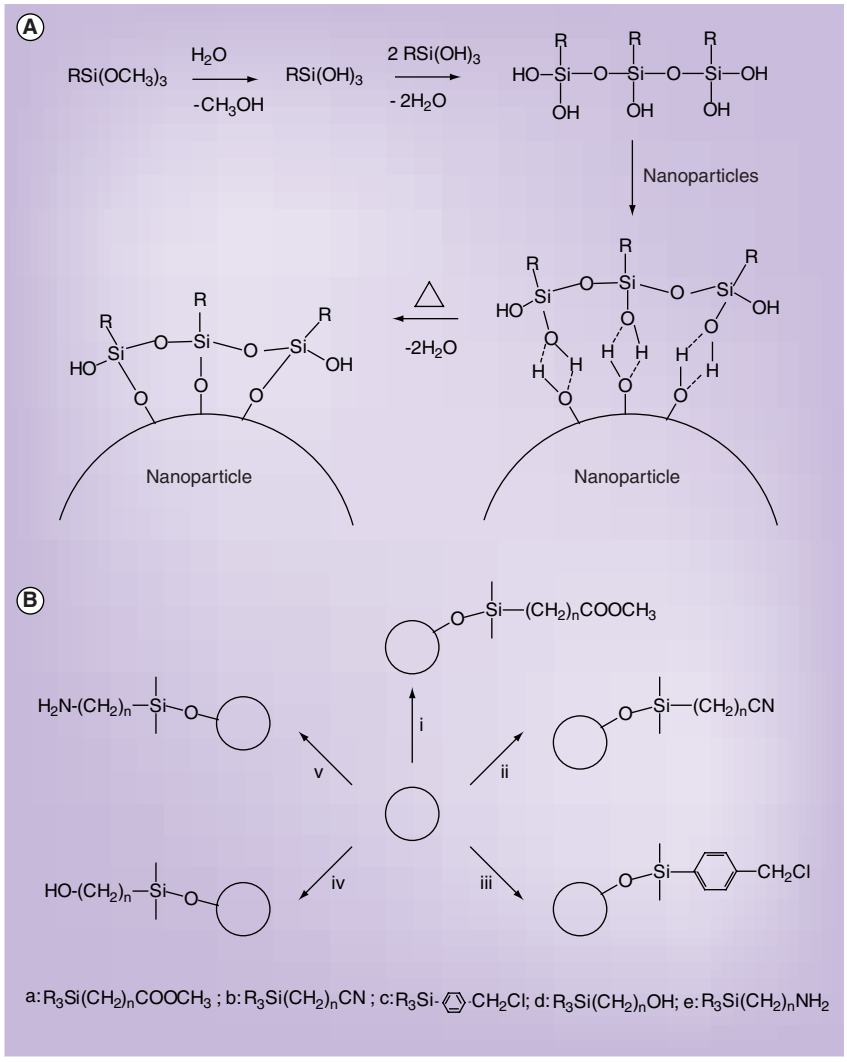


**Figure 4. (A) Adsorption mechanism of organosilane and (B) different possibilities of surface modification with organosilane.**
Adapted with permission from [1].

Magnetic resonance relaxation properties of SPIO nanoparticles have been described in a recent article [105]. Relaxation rate of iron nanoparticles clearly depends on the cluster sizes, and the evolution of the aggregation of some iron oxide particles electrostaticaly stabilized in saline media was evaluated by relaxometry [106]. A more detailed description of the relaxation technique and mechanism is presented in this article. Briefly, the size of the iron oxide particles is a major parameter in the relaxation mechanism. A cluster can be considered as a superparamagnetic sphere, where the global magnetic moment is due to the contribution of each particle that

**Table 5. Characterization techniques for the structural analysis of ferrofluids.**

| Methods of structural characterization | Main characteristics |
|---|---|
| Relaxometry | Determination of the size of the core<br>Determination of $M_{sat}$<br>Evaluation of the Néel relaxation time |
| Magnetometry | Determination of the size of the core<br>Determination of $M_{sat}$ |
| Transmission electron microscopy | Determination of the crystallinity and morphology<br>Determination of the size distribution<br>Rather long image processing (counting of a number of statistically significant particles)<br>Delicate preparation of the sample, with possible aggregation of particles → bad interpretation of the images |
| Photonic correlation spectroscopy | Determination of the hydrodynamic diameter of the particles (weighing in intensity)<br>Influenced by ionic force, viscosity, temperature and possible agglomerates |
| Mossbaüer spectroscopy | Determination of the oxide structure<br>Determination of the blocking temperature |
| X-ray diffraction | Determination of the crystalline structure of the particles<br>Cut crystalline fields<br>Impossibility of distinguishing magnetite from maghemite<br>No information on size distribution |

composed the aggregate. Concerning the characterization of colloidal iron-oxide solution, the transverse relaxation time $T_2$ is dependent on the aggregate size. During an agglomeration process, $R_2$ is modified by the agglomeration state and can be divided in three steps. During the first stage, relaxation rate is slightly or not affected and corresponds to the absence of aggregates. Sometimes, a slight diminution of the $R_2$ can be observed but it is not described by theory. It is followed by an important increase of $R_2$ until the aggregate size reaches 300 nm. For small clusters (<300 nm) the static model can be used and the translational diffusion time of the particle size $\tau_D$ is determined by the relation:

$$\tau_D = R_C^2 / D \qquad \textbf{Equation 1}$$

Where $R_C$ is the radius of the cluster and D the water diffusion coefficient. For this condition, le relaxation rate is defined by:

$$\frac{1}{T_2} = \frac{16 f_C D \omega^2 \tau_D}{45} \qquad \textbf{Equation 2}$$

Where $f_C$ is the volumic fraction of iron oxide particles in the cluster and $\Delta\omega$ is the difference in angular frequency between the magnetic field view by bulk protons and those close to the cluster. As the relaxation rate $R_2$ ($1/T_2$) depends on the square of the radius of the cluster, relaxometric measurements appear very sensitive in order to characterize the stability. In a final step, the relaxation rate $R_2$ decreases dramatically for large aggregates (>300 nm). The $\Delta\omega$ of the water proton close to such clusters is too low and the water proton diffusion in not sufficient to be affected by a fluctuation of the magnetic field. For large aggregates, the static model cannot be applied (detailed theory was described by Roch *et al.*[106]).

**Table 6. Characterization techniques for the surface analysis of ferrofluids.**

| Methods of surface characterization | Main characteristics |
|---|---|
| Infared spectroscopy (Fourier transform) | Determination of the involved species (after purification)<br>Does not allow determining the nature of the connection between the stabilizing molecule and iron oxide core |
| Potential ζ | Determination of the particle loading according to the pH<br>Determination of the PCN of ferrofluids → evaluation of ferrofluid stability<br>Influenced by pH and ionic force |
| ToF-SIM | Determination of the molecular fragments on the surface<br>High sensitivity (very weak limits of detection)<br>Depth of analysis of 1 nm → quantitative analysis<br>No information about electronic R |
| X-ray photoelectron spectroscopy | Determination of chemical environment<br>Depth analysis (6 nm) → quantitative analysis<br>Determination of the bond nature |

## Characterization

The magnetic properties of nanoparticles depend on the size and shape of the particles, the microstructure and the chemical phase. Several techniques can be used to determine the size and the chemical composition of the nanosystems **(Table 5)** or the properties of the magnetic surface of these ferrofluids **(Table 6)**. The size of the particles can be determined by transmission electron microscopy images. This technique reports the total particle size and provides details of the size distribution. X-ray diffraction can be performed to obtain the crystalline structure of the particles. The crystal size can be calculated also from the line broadening of the x-ray diffraction pattern using the Scherrer formula. Mossbauer spectroscopy is an alternative technique for assessing crystal composition. This method gives information about the order of magnitude

of the Néel relaxation time, an important characteristic of superparamagnetic particles. The PCS measurement gives a mean value of the hydrodynamic diameter of the particles. Magnetometry confirms the superparamagnetic properties of the particle and provides information on the specific magnetization and the mean diameter of the crystals. The fitting of the nuclear magentic relaxation dispersion (NMRD) curves, according to the relevant theories gives the mean crystal size, the specific magnetization and the Néel relaxation time.

## ■ Relaxivity & NMRD profiles

The NMR properties of a compound are ideally obtained by the study of its NMRD profile, which gives the evolution of relaxivity with respect to the external magnetic field [107]. The relaxivity is defined as the increase of the water relaxation rate induced by 1 mM $l^{-1}$ of iron:

$$R_{i(obs)} = \frac{1}{T_{i(obs)}} = \frac{1}{T_{i(endog)}} + r_i C;\ i = 1\ or\ 2$$

**EQUATION 3**

where $R_{i(obs)}$ and $1/T_{i(obs)}$ are the global relaxation rates of the aqueous system ($s^{-1}$), $T_{i(endog)}$ is the relaxation time of the system before addition of the contrast agent, C is the concentration of the paramagnetic centre (mM) and $r_i$ is the relaxivity ($s^{-1}mM^{-1}$).

The USPIO relaxation mechanism is built upon the original theory developed for paramagnetic systems. There are two contributions to proton relaxation: the innersphere and outersphere relaxations. Innersphere relaxation deals with the direct exchange of energy between protons and electrons located in the first hydration sphere of the paramagnetic ion and is dominated by dipolar and scalar coupling of the spins. The dipolar coupling is modulated by the rotation of the paramagnetic center $\tau_R$, the exchange rate of water molecules in and out the first hydratation sphere $\tau_M$ and the electron relaxation of the electronic spin associated with the paramagnetic ion $\tau_{S1}$. A correlation term $\tau_C$ is used to define the modulation of the dipolar couplings and is defined by:

$$\frac{1}{T_1^{IS}} = \frac{fq}{T_{1M} + \tau_M}$$

**EQUATION 4**

When scalar coupling can be neglected, the contribution of innersphere relaxation to the total relaxation rate of water protons may be predicted using the Solomon–Bloembergen equation:

$$\frac{1}{T_{IM}} = \frac{2}{15}\left(\frac{\mu_0}{4\pi}\right)^2 \gamma_H^2 \gamma_S^2 h_S^2 (S+1)\frac{1}{r^6}\left[\frac{7\tau_{c2}}{1+(\omega_S \tau_{c2})^2} + \frac{3\tau_{cl}}{1+(\omega_H \tau_{cl})^2}\right]$$

**EQUATION 5**

$$\frac{1}{\tau^{S1}} = \frac{1}{5\tau_{SO}}\left[\frac{1}{1+\omega_S^2 \tau_V^2} + \frac{4}{1+4\omega_S^2 \tau_V^2}\right]$$

**EQUATION 6**

$$\frac{1}{\tau_{S2}} = \frac{1}{10\tau_{SO}}\left[3 + \frac{5}{1+\omega_S^2 \tau_V^{\ 2}} + \frac{2}{1+4\omega_S^2 \tau_V^{\ 2}}\right]$$

**EQUATION 7**

Where f is the relative concentration of the paramagnetic complex and the water molecules, q is the number of water molecules in the first coordination sphere, $\tau_M$ is the water residence time, $\gamma_S$ and $\gamma_H$ are the gyromagnetic ratios of the electron (S) and of the proton (H), respectively; $\omega_{S,H}$ are the angular frequencies of the electron and of the proton, r is the distance between coordinated water protons and the unpaired electron spin, $\tau_{c1,2,}$ is the correlation times modulating the interaction, are defined by **EQUATION 4**, where $\tau_R$ is the rotational correlation time of the hydrated complex and $\tau_{s1,2}$ are the longitudinal and transverse relaxation times of the electron. These latter parameters are field-dependent **(EQUATIONS 7 & 8)**. $\tau_{SO}$ is the value of $\tau_{s1,2}$ at zero field and $\tau_v$ is the correlation time characteristic of the electronic relaxation times.

Outersphere relaxation arises due to the movement of the water protons near the local magnetic field gradients generated by the paramagnetic ion. The interaction between proton spins and the magnetic moment is also a dipolar interaction. This intermolecular mechanism is modulated by the diffusion time ($\tau_D$) that takes into account the relative distribution (D) between the paramagnetic center and the solvent molecule, as well as their distance of closest approach (d). The outersphere model has been described by Freed [108].

The outersphere contribution is given by:

$$R_1^{OS} = \frac{6400\pi}{81}\left(\frac{\mu_0}{4\pi}\right)^2 \gamma_H^2 \gamma_S^2 h_S^2 (s+1) NA \frac{[C]}{dD}\left[7j(\omega_S \tau_D) + 3j(\omega_H \tau_D)\right]$$

**EQUATION 8**

$$j(\omega\tau_D)\,\mathrm{Re}\left[\frac{1+\frac{1}{4}(i\omega\tau_D + \tau_D/\tau_{SI})^{1/2}}{1+(i\omega\tau_D+\tau_D/\tau_{SI})^{1/2} + \frac{4}{9}(i\omega\tau_D+\tau_D/\tau_{SI}) + \frac{1}{9}(i\omega\tau_D+\tau_D/\tau_{SI})^{3/2}}\right]$$

**EQUATION 9**

**MAGNETOMETRY**

Measurement the strength and/or direction of a magnetic field

**RELAXIVITY**

Measurement of relaxation variables in NMR and MRI

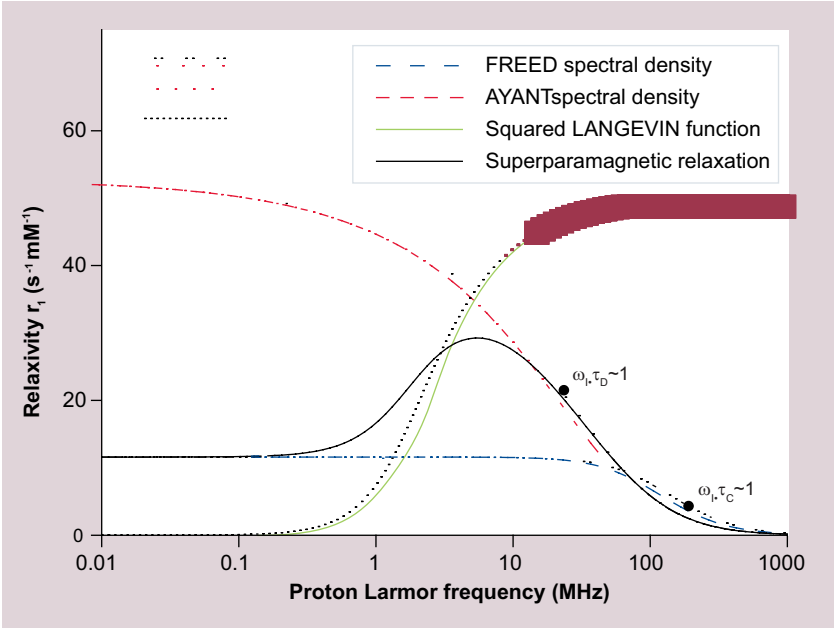


**Figure 5. Superparamagnetic model (fixed parameters: temperature = 37°C, diameter = 10 nm, Ms = 2.12 × $10^5$A/m, $\tau_N$ = 1.8 ns).**

Where d is the distance of closest approach; D is the relative diffusion coefficient, (C) is the molar concentration of the paramagnetic ion and $\tau_D = d^2/D$ is the translational correlation time.

Nuclear magnetic dispersion profiles are used to estimate the spectral density $j(\omega\tau_D)$. This density function reflects the correlation between the Larmor frequency and the electron-proton modulation, expressed as the proton relaxation rate $R_1$. The relaxation values obtained reflect the average of all interactions that influence the relaxation of water protons. The inflection points of the spectral density functions may be used to quantify physical and chemical properties of the system. In superparamagnetic colloids, the innersphere relaxation mechanism does not contribute significantly to the proton relaxation, which occurs due to the fluctuations of the dipolar magnetic coupling between the nanocrystal's magnetization and the proton spin. The relaxation is described by an OS model where the dipolar interaction fluctuates because of both the translational diffusion process and the Néel relaxation process.

The simplest model is derived when the anisotropy energy of the crystal is large enough to prevent any precession of its magnetic moment [109]. In this high anisotropy condition, the magnetization of the crystal is locked along the easy axes. The magnetic fluctuations then arise from the jumps of the moment between different easy directions according to the Néel relaxation process.

At low field, the longitudinal relaxation rate of the protons is obtained by introducing into the outersphere equations the limitation of the precession, as mentioned above: the electron Larmor precession frequency is set to zero. The spectral density function determining this component of the relaxation is then characterized by a global correlation time depending on $\tau_N$ and $\tau_D$. $\tau_N$ and $\tau_D$ are respectively the Néel relaxation time and the translation correlation time. **Figure 5** shows the dispersion of this spectral density function, known as Freed function.

For very small crystals, the assumption of a complete locking of the magnetization along the easy axes, assuming an infinite anisotropy energy, becomes less and less valid. Subsequently, the orientation of the magnetization vector out of the easy axes becomes more probable [110,111], this results in a low field dispersion **(Figure 5)**. The evaluation of the amplitude of the low-field component requires a more complete and hard theory, which takes into account the anisotropy. Note that the low field dispersion is always smaller than the one predicted by the classical paramagnetic outersphere theory. Indeed, the classical theory would be valid only for superparamagnetic colloids characterized by a null anisotropy.

At high field, the magnetic vector is locked along the external field $B_o$ and the Curie relaxation dominates. The corresponding relaxation rates are given by an outersphere model, assuming a stationary magnetization component in the $B_o$ direction and, therefore, an infinite value of the Néel relaxation time. The dispersion of this spectral density (named the Ayant function) [112] occurs when $\omega_I.\tau_D$ is approximately 1.

At intermediate field, the relaxation rates are combinations of the high field and low field contributions, weighed by factors depending on the Langevin function, which gives the average magnetization of the sample.

Thus, the classical OS theory is not applicable to these particles. A model has been proposed **(Figure 5)** that fits the NMRD experimental data and provides information regarding the nanomagnet crystals; namely, their average radius r, their specific magnetization Ms, their anisotropy energy Ea2, and their Néel relaxation time $\tau_N$.

- The average size (r): at high magnetic fields, the relaxation rate depends only on $\tau_D$ and the inflection point corresponds to the condition $\omega_I \bullet \tau_D$ at approximately 1 **(Figure 6)**.

As $\tau_D = r^2/D$, the determination of $\tau_D$ gives the crystal's size r•D and $\omega_I$ are the relative diffusion coefficient and the proton Larmor pulsation, respectively;

- The specific magnetization (Ms): at high fields, $M_s$ is approximately C $(R_{max}/\tau_D)^{1/2}$, where C is a constant and $R_{max}$ is the maximal longitudinal relaxation rate;
- The crystal anisotropy energy (Ea): the absence or presence of dispersion at low fields gives information about the magnitude of the anisotropy energy. For crystals characterized by a high Ea value, as compared with the thermal agitation, the low-field dispersion disappears;
- The Néel relaxation time ($\tau_N$): the relaxation rate at very low fields R0 is governed by a zero magnetic field correlation time τC0, which is equal to τN if τN is less than τD. Often, however, this is not the case and, so, τN is often reported as qualitative information in addition to the crystal size and the specific magnetization.

Data provided by the relaxometric techniques, together with the results obtained by magnetometry, provide a very complete description of the morphology and physical properties of a magnetic colloid. It is thus possible to determine the size of the superparamagnetic core, its saturation magnetization, the Néel relaxation time of the crystal and the values of relaxivities at different fields.

In addition to evaluating the effectiveness of the superparamagnetic particles for MRI contrast agents, relaxometry and PCS also represent invaluable tools to check the syntheses reproducibility and the stability of the colloidal solutions.

## Applications

Superparamagnetic nanoparticles are composed of a biodegradable iron oxide mineral core, which is biocompatible and can thus be recycled by cells using normal biochemical pathways for iron metabolism [113]. In addition, their surface coating allows chemical linkage of functional groups and vectorizing molecules that render them able to target a certain organ or disease [78,114].

The administration of these superparamagnetic nanoparticles to living organisms runs up against biological barriers. They are regarded as a foreign body by the mononuclear phagocyte system (MPS) [115], which tries to eliminate them from blood circulation according to a three-step mechanism:

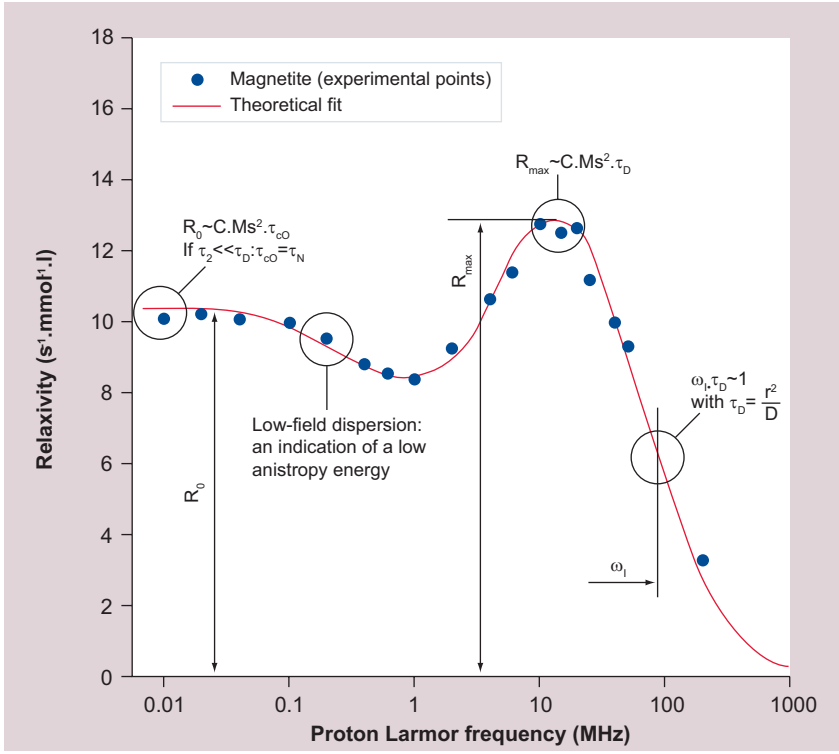


**Figure 6. Example of nuclear magentic relaxation dispersion profile of magnetite particles in colloidal solution.**

- Opsonization by plasmatic proteins;
- Recognition by the macrophages;
- Phagocytosis.

Owing to their relatively large size, their main disadvantage for MRI applications is represented by the fast opsonization after intravenous administration, which leads to a massive uptake by macrophages and mainly by the Kupffer cells in liver. They are distributed as follows: 80–90% in the liver, 5–8% in spleen and 1–2% in osseous marrow.

Due to the smaller size of USPIO, their capture by the liver macrophages is reduced. Being more furtive, they are characterized by a much longer time of plasmatic half-life: 200 min for AMI-227 and 180 min for MION-46 compared with 8 min for AMI-25 and 10 min for SHU-555.

These USPIO are particularly effective for imaging of the lymph nodes by MRI because these they are progressively taken up by macrophages in healthy lymph nodes [116].

They are able to migrate through the interstitium in a nonspecific vesicular manner to reach the lymphatic ganglia where they will be collected by the cells of the reticuloendothelial

system. The opsonization phenomenon is limited when the surface of the nanoparticles is small, neutral and hydrophilic [117].

Larger sized particles, such as SPIOs, are taken up faster than USPIO; but the charge of the coating material plays a decisive role. Hence, the blood half-life is shorter for ionic dextran (carboxy and carboxymethyl) than for nonionic dextran, while VSOP that are coated with citrate have the shortest blood half-life in humans, due to their anionic surface [78,118,119].

Small-particle ion oxide nanoparticles are well adapted for imaging of liver tumors and metastases because of the intense macrophage (Kupffer cells) uptake. Furthermore, small-sized SPIOs (7–30 nm) have optimal physicochemical and biological properties for blood-pool imaging.

One of the strategies to increase the vascular remanence of the particles is the adsorption of neutral and absorbent polymers on their surface. Polymers such as poly(ethylene oxide) or PEG have the advantage of being neutral, absorbent, bioresorbable and healthy [120]. Their grafting on the surface of the particles generates steric repulsions, making the adsorption of opsonins difficult and thus allowing an increase in the plasmatic half-life time of the injected particles [114].

Although less effective, other absorbent polymers such as dextran, polyvinyl alcohol and carboxymethyl cellulose also delay the phagocytosis of proteins since albumin does not slow down the macrophagic capture much, given the presence of negative charges in the carboxylate groups and positive charges in the amines. In all cases, the delay of the hepatic capture appears to depend on the concentration and nature of the polymer adsorbed on the particle's surface. The application of the currently available contrast agents is thus limited to the detection of tumors in bodies of the mononuclear phagocyte system such as the liver (e.g., hepatocarcinomas, lymphomas and hemangiomas), of certain pathologies, such as cirrhosis of the liver, or of inflammatory zones where the activity of the macrophages is important (e.g., cerebral attack and atherosclerosis plates). The solution consists of grafting functional groups with a specific targeting onto their surface. The most current method of vectorization [114] is to modify the nanoparticle's surface with ligands such as oligosaccharides [121], proteins [122,123] such as insulin, lactoferrin, transferrin or cerruplasmin, cholecystokinin or secretin, antibodies, peptides (RGD sequence targeting the endothelial cells), or vitamins (folic acid, vitamin B9, the receptors of which are often overexpressed in cancer cells) [124,125]. Specific recognition of these vectors by the membrane receptors leads to an internalization of the nanoparticles by the cells.

In reviews dedicated to molecular and cellular MRI topics, it has been reported that nanomolar to micromolar concentrations of the contrast agent were necessary to sufficiently increase the relaxation rates of tissue water protons and make them stand out from those in surrounding areas on the image [126,127]. However, using adequate image-acquisition parameters, the contrast effect of superparamagnetic nanoparticles is greater than that of paramagnetic compounds. Thus, the hyposignal generated by iron oxide-based contrast agents in $T_2$*-weighted MRI will occur at a lower concentration of relaxing ion than the hyperintensities arising from Gd complexes on T1-weighted images [126]. $T_2$* measurements, allowing a negative contrast enhancement due to iron oxides, are very sensitive to magnetic-field inhomogeneities, which are inducing signal voids on the image. This of course diminishes the detection specificity of such acquisition sequences in the context of cellular or molecular MRI experiments using superparamagnetic nanoparticles. Techniques for positive-contrast visualization of iron oxide-labeled cells are currently being developed [126].

**Table 7. Main biological applications for iron oxide nanoparticles.**

| Application | Necessary characteristics |
|---|---|
| MRI | High values of magnetization → high contrast → less amount to be injected<br>Non agglomerated particles characterized by a good relaxivity |
| Nonspecific cell labeling | High magnetization<br>Charged nanoparticles |
| Specific cell labeling | Vectorized nanoparticles with specific ligand for cellular receptor |
| Hyperthermia | Sharp distribution of narrow size and a magnetic diameter of 14 nm<br>High values of appear<br>Use of vectors of high specificity for the tumors |
| Drug delivery | Biodeterioration and biocompatibility of the active 'particle principle' complex<br>Adequate size to allow the transport of a sufficient amount of active drug and its diffusion through the physiological barriers<br>High values of magnetization saturation<br>Strong interactions or bonds with the drug to avoid its premature release<br>Stability of the complex under *in vivo* and *in vitro* conditions |

### ■ View of the various therapeutic strategies of superparamagnetic particles

The magnetic properties of these agents also offer interesting therapeutic prospects, including targeting by magnetic guidance, magnetic drug delivery or hyperthermia **(TABLE 7)** [6,129].

Magnetic drug delivery constitutes an attractive concept for cell therapy, because it consists in bringing the active drugs selectively to their site of action [130–132]. They can be different according to the type of therapy considered: DNA, molecules or oligonucleotides in the framework of gene vectorization or genic therapy, anticancer agents for chemotherapy or growth promoters in the case of therapy to repair lesions of the CNS. This technique makes it possible to reduce the amounts of drug and, thus, the side effects. The use of an external magnetic field, for example, allows the very concentrated maintanence of the magnetic vectors near a tumor. The release of the drug at the level of the targeted cells, tissues, or extracellular spaces must be predetermined via a strategy of coupling between the drug and the superparamagnetic nanoparticles (enzymatic rupture, sensitivity to a variation of the medium such as pH, temperature or ionic force). The magnetic properties of iron oxide also make it possible to consider another direct therapeutic application: hyperthermia [133]. This technique consists of irradiating the patient with a nonionizing electromagnetic wave in order to increase the temperature in and around the tumor. As tumorous cells are more sensitive to a contribution of external energy than healthy tissues, a selective destruction of the pathological zones can be achieved. It is necessary to reach a temperature higher than 43°C at the location of the tumor to produce a therapeutic effect [134].

Wust *et al.* showed that the use of superparamagnetic nanocrystals makes it possible to obtain a rate of transformation of magnetic energy into heat considerably higher than that obtained with ferromagnetic crystals [135]. This technique was used successfully to stop the growth of 'mammary carcinoma' tumors established on mice.

Magnetic relieving plays a capital part in the transformation of electromagnetic energy into heat. To obtain hyperthermia, the sample containing the nanomagnets is submitted to an oscillating magnetic field. The dissipation of energy is maximal when the period of oscillation of the field is of the same order of magnitude as the magnetic relaxation time of the nanomagnets [136]. Theoretical simulations showed that, for a frequency of 100 kHz, the magnetic relaxation time allowing maximum dissipation heating is estimated at $1.6 \times 10^{-6}$ s, which corresponds to a magnetite nanocrystal approximately 14 nm in diameter [137]. A major reduction in the effectiveness of the heating effect is also observed when the width of the size distribution of the particles increases. This effectiveness can be defined as the power of heating of the magnetic material per gram (specific absorption rate [SAR]).

These values are crucial for clinical trials, since the higher the SAR values, the lower the amount to inject to the patients. In addition to the size of the magnetic grain, other factors can influence the SAR values, such as the chemical composition of the particle surface and the frequency and amplitude of the magnetic field.

According to the first clinical tests [138], the combined use of thermotherapy and radiotherapy can, in certain cases, double the rate of survival after 2 years, compared with the simple radiotherapeutic treatment. Some cancers treated with chemotherapy have developed resistance to anticancer drugs used [139]. These types of cancers, refractory to chemotherapy, continue to grow, increase their blood supply and induce metastases despite the applied treatment. The use of another therapeutic system, not based on a 'chemical anticancer' could be an attractive approach. Among the proposed strategies, including hyperthermia, cell therapies appear particularly promising. Cell therapy is an alternative to the current therapeutic tools and would cover a wide field of pathology.

The cellular study of migration is one of the main applications of magnetic labeling [140]. The established stem cells appear able to migrate towards pathological zones (ischemic) and to replace the dead cells in this injured area [141]. They are regarded as therapeutic tools with great potential, in particular for the significant and difficult zones of access such as the brain or the heart. Among these, we find neuronal cells [142], spontaneous remyelination in sclerosis [143] or cell therapy of myocardial infarction [144].

To understand and optimize the use of cells, it is necessary to determine, depending on cell type used, the mechanism of cell migration and the incorporation into the damaged tissues or differentiation. Moreover, after injection, only one part of the cell population survives and an even smaller part migrates to the targeted site. Therefore, this promising strategy requires a number of optimization techniques. Currently, most investigations are

**HYPERTHERMIA**

Occurs when the body produces or absorbs more heat than it can dissipate. Hyperthermia therapy may be used to treat some kinds of tumors by elevating the body temperature

conducted by histological methods that require the sacrifice of animals and can therefore not be used in clinical cases. Thus, it is necessary to develop new imaging tools to understand, evaluate and optimize the efficiency of cell therapies. In addition to their importance in the field of molecular imaging, superparamagnetic nanoparticles are increasingly becoming essential in the field of the cellular imaging, for which the conditions are completely different. Cellular imaging process requires a nonspecific, fast and effective magnetic labeling of cells [145]. For molecular imaging, furtivity and specificity are also the key factors. The properties of the nanoparticle surface are consequently decisive for their interactions with the cells. Until now, the nanoparticles of iron oxide have been coated with dextran or albumin. However, their cell internalization remains weak. For this, cell tagging by iron oxide nanoparticles are currently investigated in order to visualize by IRM techniques the cell migrating and trafficking. There is a necessity to develop an efficient tagging protocol of cells by iron oxide particles. Arbab *et al.* (and references cited within) present an interesting background to cellular MRI for nonphagocytes cells by iron oxide nanoparticles [146]. Various techniques have been used in order to optimize cell capture. For example, cation agents of transfection such as poly-L-lysine can be added to nanoparticles to improve cellular magnetic labeling. Indeed, when they are charged, the superparamagnetic nanoparticles induce electrostatic interactions with the cellular membranes leading to the formation of blisters of endocytosis [147].

Wilhelm *et al.* also showed that the anionic maghemite nanoparticles have a high level of cellular internalization [148], comparable with that obtained for nanoparticles encapsulated in a dendrimer transfection agent [141] or combined with peptide TAT [149], resulting from a protein of virus HIV, and known for its properties of cellular penetration. Efficient labeling allows detection *in vivo* by MRI cells tagged by iron oxide nanoparticles after their intravenous injection [150].

Another strategy to increase the number of magnetic particles internalized by cells to induce a high relaxivity in order to visualize the cell trafficking leads to the use of very large particles, especially micrometer particles, as proposed by Shapiro *et al.* [151,152]. Micrometer particles can also be used as carriers for organic dyes to combine magnetic and optical imaging [153].

Labeling can also be realized *in vivo* by intravenous injection of iron oxide nanoparticles for the imaging of the inflammatory response [154], which is interesting for the study of organ rejection [155], for example. Macrophages are immunes cells that play a major role in organ rejection and their observation is mainly realized by biopsy. Following macrophages by MRI after their tagging by iron oxide nanoparticles appears very promising for the understanding of the rejection mechanism for the future transplantation success.

Contrast agents can also be built inside the cell itself. An MR reporter gene is based on this approach and it constitutes another great field of medical research [156]. A reporter gene is a gene coding for the synthesis of a contrast agent. GFP and luciferase are commonly used to study the activity of other genes for therapeutic gene delivery. An MR reporter gene is attractive because, unlike optical imaging, it presents a good anatomical resolution. The accumulation of metalloid compounds inside the cell from exogenous or endogenous sources [157,158] induces a local modification of the relaxation time and allows *in vivo* molecular imaging by MRI [159].

Magnetic particle imaging, a new tomographic imaging technique, has been developed [160,201]. This method is capable of imaging magnetic tracers at high temporal and spatial resolutions. The principle is to measure the magnetic fields generated by magnetic iron oxide nanoparticles. Researchers at Philips Research have used the technique to achieve resolutions finer than one millimeter. Magnetic particle imaging has potential applications in medicine and material science. Recently, the first *in vivo* results were published revealing structures of a beating mouse heart [161].

## Conclusion

The biological applications of these magnetic fluids, referred to in **Table 7**, are very promising. For all of them, the size, polydispersity and surface chemistry constitute three key parameters that need to be controlled in order to optimize their effectiveness and their bioselectivity. It is not conceivable, indeed, to develop only one type of particle that would be appropriate for all these applications. The great interest of this field of work focuses on the achievement of this challenge. We must develop a protocol of synthesis that allows adaption of the physicochemical characteristics of the particles according to the requirements of the biological application concerned.

Safety studies, including USPIO administration in chronic kidney disease patients on and not on dialysis, suggest that decreased kidney

function does not alter the safety profile. Thus, USPIO agents are a viable option for patients at risk for nephrogenic systemic fibrosis [162].

## Future perspective

Numerous biomedical applications have been developed that use SPIO nanoparticles: they are well adapted for imaging of liver tumors and metastases because of the intense macrophage (Kupffer cells) uptake. Another growing field of interest for medical research and clinical applications is cellular imaging, which uses superparamagnetic contrast agents to image cell migration and trafficking after transplantation. To attain the specific targeting of a pathological biomarker, the magnetic nanomaterials will be grafted to vector molecules (i.e., ligands specific for targeted receptors). The success of specific targeting with vectorized magnetic nanomaterials relies on several characteristics: a blood half-life long enough to allow an efficient interaction with targeted biomarkers, significant affinity constants to guarantee the specificity of this interaction, prolonged residence time at the targeted sites, significant enhancement of the signal/noise ratio to allow the probe detection by MRI, low toxicity, an efficient industrial synthesis and clinical implementation.

A broad diversity of ligands can be used as vector molecules, such as antibodies, peptides, polysaccharides, aptamers and synthetic mimetics. Several laboratories are particularly interested by peptide vector molecules, considering that a new facility has recently been developed locally, which is dedicated to the phage display technology. This technique has been developed during the last decade and has been used in various domains of medical research, such as the discovery of new pharmaceutical compounds and materials. The technique is based on the insertion of foreign DNA in the structural gene of a bacteriophage (recombinant DNA technology), which allows the expression of a foreign peptide at the surface of the viral envelope. The random distribution of the oligonucleotides at the level of the insert leads to the expression of a diversity of peptides (peptide library) at the surface of the viral particles. The peptides of interest are selected by incubating the library with the targeted receptor immobilized on a solid support. Subsequently, their DNA sequence is analyzed and the peptide synthesized and grafted to the magnetic reporter after an extensive biochemical characterization.

## Acknowledgements

*The authors thank Patricia de Francisco for her help in preparing the manuscript.*

## Financial & competing interests disclosure

*This work was supported by the Fonds de la Recherche Scientifique, the ARC Program 05/10-335 of the French Community of Belgium and the ENCITE program of the European Community. The support and sponsorship concerted by COST Action D38 'Metal-based Systems for Molecular Imaging Applications' and the EMIL program are kindly acknowledged.* ***The authors have no other relevant affiliations or financial involvement with any organization or entity with a financial interest in or financial conflict with the subject matter or materials discussed in the manuscript. This includes employment, consultancies, honoraria, stock ownership or options, expert testimony, grants or patents received or pending, or royalties.***

*No writing assistance was utilized in the production of this manuscript.*

## Executive summary

- A number of applications with iron oxide nanoparticles have been described and are currently in use. However, some important aspects need to be developed such as:
  - The size tuning of the nanoparticle following the chosen application.
  - The vectorization of the nanosystem surface to target a tissue or receptor, for example.
  - The surface characterization: the knowledge of the number of vectors and the determination of the affinity for the target, and the optimization of the nonspecific phagocytosis by the liver.

## Bibliography

Papers of special note have been highlighted as:
- ▪ of interest
- ▪▪ of considerable interest

1 Laurent S, Forge D, Port M *et al.* Magnetic iron oxide nanoparticles: synthesis, stabilization, vectorization, physico-chemical characterizations and biological applications. *Chem. Rev.* 108(6), 2064–2110 (2008).

▪▪ **General review on iron oxide nanoparticles with references for synthesis, physicochemical characterizations and biomedical applications**

2 Jain TK, Morales MA, Sahoo SK, Leslie-Pelecky DL, Labhasetwar V. Iron oxide nanoparticles for sustained delivery of anticancer agents. *Mol. Pharm.* 2(3), 194–205 (2005).

3 Modo MMJ, Bulte JWM. Molecular and cellular MR imaging. CRC Press, London, UK (2007).

▪▪ **Provides an overview on new developments of molecular and cellular MRI.**

4 Willard MA, Kurihara LK, Carpenter EE, Calvin S, Harris VG. Chemically prepared magnetic nanoparticles. In: *Encyclopedia of Science and Nanotechnology*. Nalwa HS (Ed.). 1, 815–848 (2004).

5 Tartaj P, Morales MP, Veintemillas-Verdaguer S, Gonzalez-Carreno T, Serna, CJ. Synthesis, properties and biomedical applications of magnetic nanoparticles. In: *Handbook of Magnetic Materials*. Buschow KHJ (Ed.). Elsevier, Amsterdam, The Netherlands 16(5), 403–482 (2006).

6 Gaviria JP, Bohé A, Pasquevich A, Pasquevich DM. Hematite to magnetite reduction monitored by Mössbauer spectroscopy and x-ray diffraction. *Physica B*. 389, 198–201 (2007).

7 Sugimoto T, Matijevic E. Formation of uniform spherical magnetite particles by crystallization from ferrous hydroxide gels. *J. Colloid Interface Sci*. 74, 227–243 (1980).

8 Massart, R. Preparation of aqueous magnetic liquids in alkaline and acidic media. *IEEE Trans. Magn*. 17, 1247–1248 (1980).

9 Martinez-Mera I, Espinosa ME, Pérez-Hernandez R, Arenas-Alatorre J. Synthesis of magnetite ($Fe_3O_4$) nanoparticles without surfactants at room temperature. *Mater. Lett.* 61, 4447–4451 (2007).

10 Hong RY, Pan TT, Han YP, Li HZ, Ding J, Han S. Magnetic field synthesis of Fe3O4 nanoparticles used as a precursor of ferrofluids. *J. Magn. Magn. Mater*. 310, 37–47 (2007).

11 Wu J-H, Ko SP, Liu H-L, Kim S, Ju JS, Kim YK. Sub 5 nm magnetite nanoparticles: synthesis, microstructure, and magnetic properties. *Mater. Lett.* 61, 3124–3129 (2007).

12 Kim DK, Zhang Y, Voit W, Rao KV, Muhammed M. Synthesis and characterization of surfactant coated superparamagnetic monodispersed iron oxide nanoparticles. *J. Magn. Magn. Mater.* 225, 30–36 (2001).

13 Gupta AK, Gupta M. Synthesis and surface engineering of iron oxide nanoparticles for biomedical applications. *Biomaterials* 26 (18), 3995–4021 (2005).

14 Husein MM, Nassar NN. Nanoparticle preparation using the single microemulsions scheme. *Curr. Nanosci.* 4(4), 370–380 (2008).

15 Hong RY, Feng B, Liu G *et al.* Preparation and characterization of $Fe_3O_4$/polystyrene composite particles via inverse emulsion polymerization. *J. Alloys Comp.* 476(1–2), 612–618 (2009).

16 López-Quintela MA, Tojo C, Blanco MC, García Rio L, Leis JR. Microemulsion dynamics and reactions in microemulsions. *Curr. Op. Colloid Interface Sci*. 9(3–4), 264–278 (2004).

17 Pileni MP, Ngo AT. Mesoscopic structures of maghemite nanocrystals: fabrication, magnetic properties, and uses. *ChemPhysChem.* 6(6), 1027–1034 (2005).

18 Lee Y, Lee J, Bae CJ *et al.* Large-scale synthesis of uniform and crystalline magnetite nanoparticles using reverse micelles as nanoreactors under reflux conditions. *Adv. Funct. Mater.* 3, 503–509 (2005).

19 Capek I. Preparation of metal nanoparticles in water-in-oil (w/o) microemulsions. *Adv. Colloid Interface Sci.* 110, 49–74 (2004).

20 Takami S, Sato T, Mousavand T, Ohara S, Umetsu M, Adschiri T. Hydrothermal synthesis of surface-modified iron oxide nanoparticles. *Mater. Lett.* 61, 4769–4772 (2007).

21 Simeonidis K, Mourdikoudis S, Moulla M *et al.* Controlled synthesis and phase characterization of Fe-based nanoparticles obtained by thermal decomposition. *J. Magn. Magn. Mater.* 316(2), E1–E4 (2007).

22 Mao B, Kang Z, Wang E *et al.* Synthesis of magnetite octahedrons from iron powders through a mild hydrothermal method. *Mater. Res. Bull.* 41, 2226–2231 (2006).

23 Tavakoli A, Sohrabi M, Kargari K. A review of methods for synthesis of nanostructured metals with emphasis on iron compounds. *Chem. Pap.* 61, 151–170 (2007).

24 Xu C, Teja AS. Continuous hydrothermal synthesis of iron oxide and PVA-protected iron oxide nanoparticles. *J. Supercrit. Fluids* 44, 85–91 (2008).

25 Tang Y, Chen Q. A simple and practical method for the preparation of magnetite nanowires. *Chem. Lett.* 36, 840–841 (2007).

26 Sun S, Zeng H, Robinson DB *et al.* Monodisperse $MFe_2O_4$ (M = Fe, Co, Mn) nanoparticles. *J. Am. Chem. Soc.* 126, 273–279 (2004).

27 Lee JS, Choi SC. Crystallization behavior of nano ceria powders by hydrothermal synthesis using a mixture of $H_2O_2$ and $NH_4OH$. *Mater. Lett.* 58, 390–393 (2004).

28 Xu J, Yang H, Fu W *et al.* Preparation and magnetic properties of magnetite nanoparticles by sol–gel method. *J. Magn. Magn. Mater.* 309, 307–311 (2007).

29 Clapsaddle BJ, Gash AE, Satcher JH, Simpson RL. Silicon oxide in an iron(III) oxide matrix: the sol–gel synthesis and characterization of Fe–Si mixed oxide nanocomposites that contain iron oxide as the major phase. *J. Non-Cryst. Solids* 331, 190–201 (2003).

30 Nagineni VS, Zhao SH, Potluri A *et al.* Microreactors for syngas conversion to higher alkanes. characterization of sol-gel-encapsulated nanoscale Fe-Co catalysts in the microchannels. *Ind. Eng. Chem. Res.* 44, 5602–5607 (2005).

31 Jitianu A, Raileanu M, Crisan M *et al.* $Fe_3O_4$-$SiO_2$ nanocomposites obtained via alkoxide and colloidal route. *J. Sol-Gel Sci. Techn*. 40, 317–323 (2006).

32 Dong J, Xu ZH, Wang F. Engineering and characterization of mesoporous silica-coated magnetic particles for mercury removal from industrial effluents. *Appl. Surf. Sci*. 254, 3522–3530 (2008).

33 Park ME, Chang JH. High throughput human DNA purification with aminosilanes tailored silica-coated magnetic nanoparticles. *Mater. Sci. Eng. C* 27, 1232–1235 (2007).

34 Stöber W, Fink A, Bohn E. Controlled growth of monodisperse silica spheres in the micron size range. *J. Colloid Interf. Sci.* 26, 62–69 (1968).

35 Vasquez M, Luna C, Morales MP, Sanz R, Serna CJ, Mijangos C. Magnetic nanoparticles: synthesis, ordering and properties. *Physica B.* 354, 71–79 (2004).

36 Liu HL, Ko SP, Wu JH *et al.* One-pot polyol synthesis of monosize PVP-coated sub-5 nm $Fe_3O_4$ nanoparticles for biomedical applications. *J. Magn. Magn. Mater.* 310, E815–E817 (2007).

37 Caruntu D, Caruntu G, Chen Y, O'Connor CJ, Goloverda G, Kolesnichenko VL. Synthesis of variable-sized nanocrystals of $Fe_3O_4$ with high surface reactivity. *Chem. Mater.* 16, 5527–5534 (2004).

38 Cai W, Wan J. Facile synthesis of superparamagnetic magnetite nanoparticles in liquid polyols. *J. Colloid Interface Sci.* 305, 366–370 (2007).

39 Varadwaj KS, Ghose J. Synthesis and characterisation of polyol-capped transition metal oxide nanoparticles. *J. Nanosci. Nanotechnol.* 5(4), 627–634 (2005).

40 Kim EH, Ahn Y, Lee HS. Biomedical applications of superparamagnetic iron oxide nanoparticles encapsulated within chitosan. *J. Alloys Compd*. 434, 633–636 (2007).

41 Pinkas J, Reichlova V, Zboril R, Moravec Z, Bezdicka P, Matejkova J. Sonochemical synthesis of amorphous nanoscopic iron(III) oxide from $Fe(acac)_3$. *Ultrason. Sonochem*. 15, 257–264 (2008).

42 Haas I, Gedanken A. Sonoelectrochemistry of $Cu^{++}$ in the presence of CTAB: obtaining instead of copper. *Chem. Mater.* 18, 1184–1189 (2006).

43 Morel AL, Nikitenko SI, Gionnet K *et al.* Sonochemical approach to the synthesis of $Fe_3O_4$@$SiO_2$ core-shell nanoparticles with tunable properties. *ACS Nano.* 2(5), 847–856 (2008).

44 Abu-Much R, Meridor U, Frydman A, Gedanken A. The formation of a 3D microstructure of $Fe_3O_4$-PVA composite by evaporating the hydrosol under a magnetic field. *J. Phys. Chem. B* 110, 8194–8203 (2006).

45 Kim EH, Lee HS, Kwak BK, Kim BK. Synthesis of ferrofluid with magnetic nanoparticles by sonochemical method for MRI contrast agent. *J. Magn. Magn. Mater.* 289, 328–330 (2005).

46 Khalil H, Mahajan D, Rafailovich M, Gelfer M, Pandya K. Synthesis of nanophase metal particles stabilized with polyethylene glycol. *Langmuir* 20, 6896–6903 (2004).

47 David B, Pizurova N, Schneeweiss O, Bezdicka P, Morjan I, Alexandrescu R. Preparation of iron/graphite core-shell structured nanoparticles. *J. Alloys Compd* 378, 112–116 (2004).

48 Jana NR, Chen YF, Peng XG. Size- and shape-controlled magnetic (Cr, Mn, Fe, Co and Ni) oxide nanocrystals via a simple and general approach. *Chem. Mater.* 16, 3931–3935 (2004).

49 Basak S, Chen D-R, Biswas P. Electrospray of ionic precursor solutions to synthesize iron oxide nanoparticles: modified scaling law. *Chem. Eng. Sci. 62,* 1263–1268 (2007).

50 Bomati- Miguel O, Morales MP, Tartaj P *et al.* Fe-based nanoparticulate metallic alloys as contrast agents for magnetic resonance imaging. *Biomaterials* 26, 5695–5703 (2005).

51 Tartaj P, Gonzáles-Carreño T, Serna CJ. From hollow to dense spheres: control of dipolar interactions by tailoring the architecture in colloidal aggregates of superparamagnetic iron oxide nanocrystals. *Adv. Mater.* 16, 529–533 (2004).

52 Jolivet JP, Cassaignon S, Chanéac C, Chiche D, Tronc E. Design of oxide nanoparticles by aqueous chemistry. *J. Sol-Gel Sci. Techn.* 46(3), 299–305 (2008).

53 Hu S-H, Liu D-M, Tung W-L, Liao C-F, Chen S-Y. Surfactant-free, self-assembled PVA-iron oxide/silica core-shell nanocarriers for highly sensitive, magnetically controlled drug release and ultrahigh cancer cell uptake efficiency. *Adv. Funct. Mater. 18(19), 2946–2955 (2008).*

54 Jarrett BR, Frendo M, Vogan J, Louie AY. Size-controlled synthesis of dextran sulfate coated iron oxide nanoparticles for magnetic resonance imaging. *Nanotechnology* 18(3), 18–24 (2007).

55 Gupta AK, Wells S. Surface-modified superparamagnetic nanoparticles for drug delivery: preparation, characterization, and cytotoxicity studies. *IEEE Trans. Nanobioscience* 3, 66–73 (2004).

▪ **Emphasizes the cytotoxicity of nanoparticles.**

56 Albornoz C, Jacobo SE. Preparation of a biocompatible magnetic film from an aqueous ferrofluid. *J. Magn. Magn. Mater.* 305, 12–15 (2006).

57 Wassel RA, Grady B, Kopke RD, Dormer KJ. Dispersion of super paramagnetic iron oxide nanoparticles in poly(D,L-lactide-co-glycolide) microparticles. *Colloids Surf. A Physicohem. Eng. Aspects* 92, 125–130 (2007).

58 Mak S, Chen D. Binding and sulfonation of poly(acrylic acid) on iron oxide nanoparticles. *Macro-mol. Rapid Comm.* 26, 1567–1571 (2005).

59 Arias JL, Gallardo V, Gomez-Lopera SA, Delgado AV. Loading of 5-fluorouracil to poly(ethyl-2-cyanoacrylate) nanoparticles with a magnetic core. *J. Biomed. Nanotech.* 1, 214–223 (2005).

60 Berret JF, Oberdisse J. Electrostatic self-assembly in polyelectrolyte-neutral block copolymers and oppositely charged surfactant solutions. *Physica B* 350, 204–206 (2004).

61 Kumagai M, Imai Y, Nakamura T *et al.* Iron hydroxide nanoparticles coated with poly(ethylene glycol)-poly(aspartic acid) block copolymer as novel magnetic resonance contrast agents for *in vivo* cancer imaging. *Colloids Surf. B Biointerfaces* 56, 174–181 (2007).

62 Akcora P, Zhang X, Varughese B, Briber RM, Kofinas P. Structural and magnetic characterization of norbornene-deuterated norbornene dicarboxylic acid diblock copolymers doped with iron oxide nanoparticles. *Polymer* 46, 5194–5201 (2005).

63 Gamarra LF, Brito GES, Pontuschka WM, Amaro E, Parma AHC, Goya GF. Biocompatible superparamagnetic iron oxide nanoparticles used for contrast agents: a structural and magnetic study. *J. Magn. Magn. Mater.* 289, 439–441 (2005).

64 Molday RS, MacKenzie D. Immunospecific ferromagnetic iron-dextran reagents for the labeling and magnetic separation of cells. *J. Immunol. Meth.* 52, 353–367 (1982).

65 Laurent S, Nicotra C, Gossuin Y *et al.* Influence of the length of the coating molecules on the nuclear magnetic relaxivity of superparamagnetic colloids. *Phys. Stat. Sol.* 12, 3644–3650 (2004).

66 Mejías R, Costo R, Roca AG *et al.* Cytokine adsorption/release on uniform magnetic nanoparticles for localized drug delivery. *J. Control. Release* 130(2), 168–174 (2008).

67 Li W, Tutton S, Vu AT *et al.* First-pass contrast-enhanced magnetic resonance angiography in humans using ferumoxytol a novel ultrasmall superparamagnetic iron oxide USPIO-based blood pool agent. *J. Magn. Reson. Imaging* 21, 46–52 (2005).

68 Nishio Y, Yamada A, Ezaki K, Miyashita Y, Furukawa H, Horie K. Preparation and magnetometric characterization of iron oxide-containing alginate/poly(vinyl alcohol) networks. *Polymer* 45, 7129–7136 (2004).

69 Janardhanan SR, Ramasamy I, Nair BU. Synthesis of iron oxide nanoparticles using chitosan and starch templates. *Trans. Metal Chem.* 33(1), 127–131 (2008).

70 Yonezawa T, Kamoshita K, Tanaka M, Kinoshita T. Easy preparation of stable iron oxide nanoparticles using gelatin as stabilizing molecules. *Jap. J. Appl. Phys.* 47(2), 1389–1392 (2008).

71 Rekha MR, Sharma CP. Pullulan as a promising biomaterial for biomedical applications: a perspective. *Trends Biomater. Artif. Organs* 20(2), 116–121 (2007).

72 Shultz MD, Calvin S, Fatouros PP, Morrison SA, Carpenter EE. Enhanced ferrite nanoparticles as MRI contrast agents. *J. Magn. Magn. Mater.* 311, 464–468 (2007).

73 Wassel RA, Grady B, Kopke RD, Dormer KJ. Dispersion of superparamagnetic iron oxide nanoparticles in poly(D,L-lactide-co-glycolide) microparticles. *Colloids Surf. A Physicochem. Eng. Aspects* 292, 125–130 (2007).

74 Finotelli PV, Morales MA, Rocha-Leão MH, Baggio-Saitovitch EM, Rossi AM. Magnetic studies of iron(III) nanoparticles in alginate polymer for drug delivery applications. *Mater. Sci. Eng. C Biomin. Mater. Sens. Syst.* 24, 625–629 (2004).

75 Iijima M, Yonemochi Y, Tsukada M, Kamiya H. Microstructure control of iron hydroxide nanoparticles using surfactants with different molecular structures. *J. Colloid Interf. Sci.* 298, 202–208 (2006).

76 Xu ZZ, Wang CC, Yang WL, Deng YH, Fu SK. Encapsulation of nanosized magnetic iron oxide by polyacrylamide via inverse miniemulsion polymerization. *J. Magn. Magn. Mater.* 277(1–2), 136–143 (2004).

77 Ma Y-H, Wu S-Y, Wu T, Chang Y-J, Hua M-Y, Chen J-P. Magnetically targeted thrombolysis with recombinant tissue plasminogen activator bound to polyacrylic acid-coated nanoparticles. *Biomaterials* 30(19), 3343–3351 (2009).

78 Bae S-J, Park J-A, Lee J-J *et al.* Ultrasmall iron oxide nanoparticles: synthesis, physicochemical, and magnetic properties. *Curr. Appl. Phys.* 9(Suppl. 1), S19–S21 (2009).

79 Gomez-Lopera SA, Arias JL, Gallardo V, Delgado AV. Colloidal stability of magnetite/poly(lactic acid) core/shell nanoparticles. *Langmuir* 22, 2816–2821 (2006).

80 Arias JL, Lopez-Viota M, Ruiz MA, Lopez-Viota J, Delgado AV. Development of carbonyl iron/ethylcellulose core/shell nanoparticles for biomedical applications. *Int. J. Pharm.* 339, 237–245 (2007).

81 Flesch C, Bourgeaut-Lami E, Mornet S, Duguet E, Delaite C, Dumas P. Synthesis of colloidal superparamagnetic nanocomposites by grafting poly(ε-caprolactone) from the surface of organosilane-modified maghemite nanoparticles. *J. Polym. Sci. Part A: Polym. Chem*. 43, 3221–3231 (2005).

82 Corot C, Robert P, Idée J-M, Port M. Recent advances in iron oxide nanocrystal technology for medical imaging. *Adv. Drug Del. Rev.* 58(14), 1471–1504 (2006).

83 Huang Z, Tang F. Preparation, structure, and magnetic properties of polystyrene coated by $Fe_3O_4$ nanoparticles. *J. Colloid Interface Sci*. 275, 142–147 (2004).

84 Aphesteguy JC, Jacobo SE. Composite of polyaniline containing iron oxides. *Physica B*. 354, 224–227 (2004).

85 Butter K, Kassapidou K, Vroege GJ, Philipse AP. Preparation and properties of colloidal iron dispersions. *J. Colloid Interface Sci.* 287, 485–495 (2005).

86 Zhang L, He R, Gu HC. Oleic acid coating on the monodisperse magnetite nanoparticles. *Appl. Surf. Sci.* 253, 2611–2617 (2006).

87 Khalafalla SE, Reimers GW. Preparation of dilution-stable aqueous *magnetic* fluids. *IEEE Trans. Magn.* 16, 178–183 (1980).

88 Bonacchi D, Caneschi A, Gatteschi D, Sangregorio C, Sessoli R, Falqui A. Synthesis and characterisation of metal oxides nanoparticles entrapped in cyclodextrin. *J. Phys. Chem. Solids* 65(4), 719–722 (2004).

89 Gonzales M, Krishnan KM. Phase transfer of highly monodisperse iron oxide nanocrystals with Pluronic F127 for biomedical applications. *J. Magn. Magn. Mater.* 311, 59–62 (2007).

90 Kim EH, Lee HS, Kwak BK, Kim BK. Synthesis of ferrofluid with magnetic nanoparticles by sonochemical method for MRI contrast agent. *J. Magn. Magn. Mater.* 289, 328–330 (2005).

91 Sahoo Y, Goodarzi A, Swihart MT *et al.* Aqueous ferrofluid of magnetite nanoparticles. fluorescence labeling and magnetophoretic control. *J. Phys. Chem. B.* 109, 3879–3885 (2005).

▪ **Uses nanoparticles as MRI contrast agents and as fluorescent probes.**

92 Taupitz M, Wagner S, Schnorr J *et al.* Phase I clinical evaluation of citrate-coated monocrystalline very small superparamagnetic iron oxide particles as a new contrast medium for magnetic resonance imaging. *Invest. Radiol.* 39, 394–405 (2004).

93 Mohapatra S, Pramanik N, Ghost SK, Pramanik PJ. Synthesis and characterization ultrafine poly(vinylalcohol phosphate) coated magnetite nanoparticles. *Nanosci. Nanotechnol.* 6, 823–829 (2006).

94 Daou TJ, Buathong S, Ung D *et al.* Investigation of the grafting rate of organic molecules on the surface of magnetite nanoparticles as a function of the coupling agent. *Sens. Actuators B* 126(1), 159–162 (2006).

95 Roux S, Garcia B, Bridot JL *et al.* Synthesis, characterization of dihydrolipoic acid capped gold nanoparticles, and functionalization by the electroluminescent luminol. *Langmuir* 21, 2526–2536 (2005).

96 Saini G, Shenoy D, Nagesha DK, Kautz R, Sridhar S, Amiji M. Superparamagnetic iron oxide–gold core–shell nanoparticles for biomedical applications. In: *Technical Proceedings of the 2005 NSTI Nanotechnology Conference and Trade Show, Volume 1, BioNano Materials* 328–331 (2005).

97 Choi K-H, Lee S-H, Kim Y-R *et al.* Magnetic behavior of $Fe_3O_4$ nanostructure fabricated by template method. *J. Magn. Magn. Mater.* 310, e861-e863 (2007).

98 Zhang M, Cushing BL, O'Connor CJ. Synthesis and characterization of monodisperse ultra-thin silica-coated magnetic nanoparticles. *Nanotechnology* 19, 1–5 (2008).

99 Alcala MD, Real C. Synthesis based on the wet impregnation method and characterization of iron and iron oxide-silica nanocomposites. *Solid State Ionics* 177, 955–960 (2006).

100 Ma D, Guan J, Normandin F *et al.* Multifunctional nano-architecture for biomedical applications. *Chem. Mater.* 18, 1920–1927 (2006).

101 Sun Y, Duan L, Guo Z *et al.* An improved way to prepare superparamagnetic magnetite-silica core-shell nanoparticles for possible biological application. *J. Magn. Magn. Mater.* 285, 65–70 (2005).

102 Liu XQ, Xing J, Guan Y, Shan G, Liu HZ. Synthesis of amino-silane modified superparamagnetic silica supports and their use for protein immobilization. *Colloids Surf. A: Physicochem. Eng. Aspects* 238, 127–131 (2004).

103 Barnakov YA, Yu MH, Rosenzweig Z. Manipulation of the magnetic properties of magnetite-silica nanocomposite materials by controlled Stober synthesis. *Langmuir* 21, 7524–7527 (2005).

104 Nobbmann U, Morfesis A. Light scattering and nanoparticles. *Material today* 12, 52–54 (2009).

105 Gossuin Y, Gillis P, Hocq A, Vuong QL, Roch A. MR relaxation properties of superparamagnetic iron oxide particles. *Nanomed. Nanobiotechnol.* 1, 299–310 (2008).

106 Roch A, Gossuin Y, Muller R N, Gillis P. Superparamagnetic colloid suspensions: water magnetic relaxation and clustering. *J. Magn. Magn. Mater.* 293, 532–539 (2005).

107 Laurent S, Vander Elst L, Muller RN. Contrast agents for MRI: recent advances. In: *Encyclopedia of Magnetic Resonance.* Harris RK, Wasylishen R (Eds). John Wiley, Chichester, UK (2009).

▪▪ **Provides a comparison between Gd complexes and nanoparticles as MRI contrast agents.**

108 Freed JH. Dynamic effects of pair correlation functions on spin relaxation by translational diffusion in liquids. *J. Chem. Phys.* 68, 4034–4037 (1978).

109 Roch A, Muller RN, Gillis P. Water relaxation by SPM particles: neglecting the magnetic anisotropy? A caveat. *J. Magn. Reson. Imaging* 14, 94–96 (2001).

110 Roch A, Muller RN, Gillis P. Theory of proton relaxation induced by superparamagnetic particles. *J. Chem. Phys.* 110, 5403–5411 (1999).

111 Roch A, Gillis P, Ouakssim A, Muller RN. Proton relaxation in superparamagnetic aqueous colloids: a new tool for the investigation of ferrite crystal anisotropy. *J. Magn. Magn. Mater.* 201, 77–79 (1999)

112 Ayant Y, Belorizly E, Alizon J, Gallice J. Calculation of spectral density resulting from random translational movement with relaxation by magnetic dipolar interaction in liquids. *J. Phys.* 36, 991–1004 (1975).

113 Bulte JWM, Kraitchman DL. Iron oxide MR contrast agents for molecular and cellular imaging. *NMR Biomed.* 17, 484–499 (2004).

114 Thorek DLJ, Chen AK, Czupryna J, Tsourkas A. Superparamagnetic iron oxide nanoparticle probes for molecular imaging. *Ann. Biomed. Eng.* 34, 23–38 (2006).

115 Owens DE, Peppas NA. Opsonization, biodistribution, and pharmacokinetics of polymeric nanoparticles. *Int. J. Pharm.* 307, 93–102 (2006).

116 Pultrum BB, van der Jagt EJ, van Westreenen HL *et al.* Detection of lymph node metastases with ultrasmall

superparamagnetic iron oxide (USPIO)-enhanced magnetic resonance imaging in oesophageal cancer. A feasibility study. *Cancer Imaging* 9, 19–28 (2009).

117 Yoo HJ, Lee JM, Lee MW *et al.* Hepatocellular carcinoma in cirrhotic liver: double-contrast-enhanced, high-resolution 3.0 T-MR imaging with pathologic correlation. *Invest. Radiol.* 43(7), 538–546 (2008).

118 Thorek DL, Tsourkas A. Size, charge and concentration dependent uptake of iron oxide particles by non-phagocytic cells. *Biomaterials* 29(26), 3583–3590 (2008).

119 Sun R, Dittrich J, Le-Huu M *et al.* Physical and biological characterization of superparamagnetic iron oxide- and ultrasmall superparamagnetic iron oxide-labeled cells: a comparison. *Invest Radiol.* 40(8), 504–513 (2005).

120 Kohler N, Fryxell GE, Zhang M. A bifunctional poly(ethylene glycol) silane immobilized on metallic oxide-based nanoparticles for conjugation with cell targeting agents. *J. Am. Chem. Soc.* 126, 7206–7211 (2004).

121 Mornet S, Vasseur S, Grasset F *et al.* Magnetic nanoparticle design for medical applications. *Progress Solid State Chem.* 34(2–4), 237–247 (2006).

122 Kou G, Wang S, Cheng C *et al.* Development of SM5-1-conjugated ultrasmall superparamagnetic iron oxide nanoparticles for hepatoma detection. *Biochem. Biophys. Res. Commun.* 374(2), 192–197 (2008).

123 Burtea C, Laurent S, Vander Elst L, Muller RN. C-MALISA (cellular magnetic-linked immunosorbent assay), a new application of cellular ELISA for MRI. *J. Inorg. Biochem.* 99(5), 1135–1144 (2005).

124 Boutry S, Laurent S, Vander Elst L, Muller RN. Specific E-selectin targeting with a superparamagnetic MRI contrast agent. *Contrast Med. Mol. Imaging* 1(1), 15–22 (2006).

125 Di Marco M, Sadun C, Port M, Guilbert I, Couvreur P, Dubernet C. Physicochemical characterization of ultrasmall superparamagnetic iron oxide particles (USPIO) for biomedical application as MRI contrast agents. *Int. J. Nanomedicine* 2(4), 609–622 (2007).

▪ **Describes a complete physicochemcial characterization of ultrasmall superparamagnetic iron oxide nanoparticles before biomedical application.**

126 Liu W, Frank JA. Detection and quantification of magnetically labeled cells by cellular MRI. *Eur. J. Radiol.* 70, 258–264 (2009).

127 Bulte JWM, Kraitchman DL. Iron oxide MR contrast agents for molecular and cellular imaging. *NMR Biomed.* 17, 484–499 (2004).

128 Mills PH, Ahrens ET. Enhanced positive-contrast visualization of paramagnetic contrast agents using phase images. *Magn. Reson. Med.* 62(5), 1349–1355 (2009).

129 Nelson GN, Roh JD, Mirensky TL *et al.* Initial evaluation of the use of USPIO cell labeling and noninvasive MR monitoring of human tissue-engineered vascular grafts *in vivo*. *FASEB J.* 22, 3888–3895 (2008).

130 Douziech-Eyrolles L, Marchais H, Hervé K *et al.* Nanovectors for anticancer agents based on superparamagnetic iron oxide nanoparticles. *Int. J. Nanomed.* 2(4), 541–550 (2007).

131 Cengelli F, Grzyb JA, Montoro A, Hofmann H, Hanessian S, Juillerat-Jeanneret L. Surface-functionalized ultrasmall superparamagnetic nanoparticles as magnetic delivery vectors for camptothecin. *ChemMedChem.* 4(6), 988–997 (2009).

132 Sajja HK, East MP, Mao H, Wang YA, Nie S, Yang L. Development of multifunctional nanoparticles for targeted drug delivery and noninvasive imaging of therapeutic effect. *Curr. Drug Discov. Technol.* 6(1), 43–51 (2009).

133 Purushotham S, Chang PE, Rumpel H *et al.* Thermoresponsive core-shell magnetic nanoparticles for combined modalities of cancer therapy. *Nanotechnology* 20(30), 5101 (2009).

134 Renard PE, Buchegger F, Petri-Fink A *et al.* Local moderate magnetically induced hyperthermia using an implant formed *in situ* in a mouse tumor model. *Int. J. Hyperthermia* 25(3), 229–239 (2009).

135 Wust P, Gneveckow U, Johannsen M *et al.* Magnetic nanoparticles for interstitial thermotherapy- feasibility, tolerance and achieved temperatures. *Int. J. Hyperthermia* 22(8), 673–685 (2006).

136 Fortin JP, Wilhelm C, Servais J, Ménager C, Bacri JC, Gazeau F. Size-sorted anionic iron oxide nanomagnets as colloidal mediators for magnetic hyperthermia. *J. Am. Chem. Soc.* 129, 2628–2635 (2007).

137 Rosenweig RE. Heating magnetic fluid with alternating magnetic field. *J. Magn. Magn. Mater.* 252, 370–374 (2002).

138 Maier-Hauff K, Rothe R, Scholz R *et al.* Intracranial thermotherapy using magnetic nanoparticles combined with external beam radiotherapy. results of a feasibility study on patients with glioblastoma multiforme. *J. Neurooncol.* 81(1), 53–60 (2007).

139 Szakacs G, Paterson JK, Ludwig JA, Booth-Genthe C, Gottesman MM. Targeting multidrug resistance in cancer, *Nat. Rev. Drug Discov.* 5, 219–234 (2006).

140 Bulte JW. Intracellular endosomal magnetic labeling of cells. *Methods Mol. Med.* 124, 419–439 (2006).

141 Jing Y, Mal N, Williams PS *et al.* Quantitative intracellular magnetic nanoparticle uptake measured by live cell magneto-phoresis. *FASEB J.* 22(12), 4239–4247 (2008).

142 Delcroix GJ, Jacquart M, Lemaire L *et al.* Mesenchymal and neural stem cells labeled with HEDP-coated SPIO nanoparticles. *in vitro* characterization and migration potential in rat brain. *Brain Res.* 1255, 18–31 (2009).

143 Pluchino S, Martino G. The therapeutic use of stem cells for myelin repair in autoimmune demyelinating disorders. *J. Neurol. Sci.* 233, 117–119 (2005).

144 Klabusay M, Scheer P, Doubek M, Rehakova K, Coupek P, Horky D. Retention of nanoparticle-labeled bone marrow mononuclear cells in the isolated *ex vivo* perfused heart after myocardial infarction in animal model. *Exp. Biol. Med. (Maywood).* 234(2), 222–231 (2009).

145 Billotey C, Aspord C, Beuf O *et al.* T-cell homing to the pancreas in autoimmune mouse models of diabetes. *in vivo* MR imaging. *Radiology* 236, 579–587 (2005).

146 Arbab AS, Liu W, Frank JA. Cellular magnetic resonance imaging. current status and future prospects *Expert Rev. of Med. Devices* 3, 427–439 (2006).

147 Chen CB, Chen JY, Lee WC. Fast transfection of mammalian cells using superparamagnetic nanoparticles under strong magnetic field. *J. Nanosci. Nanotechnol.* 9(4), 2651–2659 (2009).

148 Wilhelm C, Gazeau F. Magnetic nanoparticles: internal probes and heaters within living cells. *J. Magn. Magn. Mater.* 321, 671–674 (2009).

149 Morgul MH, Raschzok N, Schwartlander R *et al.* Tracking of primary human hepatocytes with clinical MRI: initial results with Tat-peptide modified superparamagnetic iron oxide particles. *Int. J. Artif. Organs* 31(3), 252–257 (2008).

150 Heyn C, Ronald JA, Mackenzie LT *et al.* *In vivo* magnetic resonance imaging of single cells in mouse brain with optical validation. *Magn. Reson. Med.* 55, 23–29 (2006).

151 Shapiro EM, Skrtic S, Koretsky AP. Sizing it up. Cellular MRI using micron-sized iron oxide particles. *Magn. Reson. Med.* 53, 329–338 (2005).

152 Shapiro EM, Sharer K, Skrtic S, Koretsky AP. *In vivo* detection of single cells by MRI. *Magn. Reson. Med.* 55, 242–249 (2006).

153 Sumner JP, Conroy R, Shapiro EM, Moreland J, Koretsky AP. Delivery of fluorescent probes using iron oxide particles as carriers enables *in vivo* labeling of migrating neural precursors for magnetic resonance imaging and optical imaging. *J. Biomed. Optics* 12, 051504–051506 (2007).

154 Dunn EA, Weaver LC, Dekaban GA, Foster PJ. Cellular imaging of inflammation after experimental spinal cord injury. *Mol. Imaging* 4(1),53–62 (2005).

155 Wu YL, Ye Q, Foley LM *et al. In situ* labeling of immune cells with iron oxide particles. An approach to detect organ rejection by cellular MRI. PNAS, 103, 1852–1857 (2006).

156 Gilad AA, Winnard PT Jr, van Zijl PCM, Bulte JWM. Developing MR reporter genes. promises and pitfalls. *NMR Biomed.* 20, 275–290 (2007).

157 Genove G, DeMarco U, Xu H, Goins WF, Ahrens ET. A new transgene reporter for *in vivo* magnetic resonance imaging. *Nature Med.* 11, 450–454 (2005).

158 Batya C, Hagit D, Gila M, Alon H, Michal N. Ferritin as an endogenous MRI reporter for noninvasive imaging of gene expression in C6 glioma tumors. *Neaplasia* 7, 109–117 (2005).

159 Cohen B, Ziv K, Plaks V *et al.* MRI detection of transcriptional regulation of gene expression in transgenic mice. *Nature Med.* 13, 498–503 (2007).

160 Rahmer J, Weizenecker J, Gleich B, Borgert J. Signal encoding in magnetic particle imaging: properties of the system function. *BMC Medical Imaging* 9(4), 1–21 (2009).

161 Weizenecker J, Gleich B, Rahmer J, Dahnke H, Borgert J. Three-dimensional real-time *in vivo* magnetic particle Imaging *Phys. Med. Biol.* 54(5), L1–L10 (2009).

162 Neuwelt EA, Hamilton BE, Varallyay CG, *et al.* Ultrasmall superparamagnetic iron oxides (USPIOs). a future alternative magnetic resonance (MR) contrast agent for patients at risk for nephrogenic systemic fibrosis (NSF)? *Kidney Int.* 75(5), 465–474 (2009).

▪ **Demonstrates that iron oxide nanoparticles can be injected to patients with risk for nephrogenic systemic fibrosis.**

163 Modo M, Hoehn M, Bulte JW. Cellular MR imaging. *Mol. Imaging* 4, 143–164 (2005).

164 Weinmann HJ, Ebert W, Misselwitz B, Schmitt-Willich H. Tissue-specific MR contrast agents. *Eur. J. Radiol.* 46, 33–44 (2003).

165 Wang YX, Hussain SM, Krestin GP. Superparamagnetic iron oxide contrast agents: physicochemical characteristics and applications in MR imaging. *Eur. Radiol.* 11, 2319–2331 (2001).

166 Muldoon LL, Sandor M, Pinkston KE, Neuwelt EA. Imaging, distribution, and toxicity of superparamagnetic iron oxide magnetic resonance nanoparticles in the rat brain and intracerebral tumor. *Neurosurgery* 57, 785–796 (2005).

167 Simon GH, von Vopelius-Feldt J, Fu Y *et al.* Ultrasmall supraparamagnetic iron oxide-enhanced magnetic resonance imaging of antigen-induced arthritis. a comparative study between SHU 555 C, ferumoxtran-10, and ferumoxytol. *Invest. Radiol.* 41, 45–51 (2006).

168 Sun R, Dittrich J, Le-Huu M *et al.* Physical and biological characterization of superparamagnetic iron oxide- and ultrasmall superparamagnetic iron oxide-labeled cells. a comparison. *Invest. Radiol.* 40, 504–513 (2005).

169 Matuszewski L, Persigehl T, Wall A *et al.* Cell tagging with clinically approved iron oxides. feasibility and effect of lipofection, particle size, and surface coating on labeling efficiency. *Radiology* 235, 155–161 (2005).

170 Wacker FK, Reither K, Ebert W, Wendt M, Lewin JS, Wolf KJ. MR image-guided endovascular procedures with the ultrasmall superparamagnetic iron oxide SH U 555 C as an intravascular contrast agent: study in pigs. *Radiology* 226, 459–464 (2003).

171 Li W, Tutton S, Vu AT *et al.* Firstpass contrast-enhanced magnetic resonance angiography in humans using ferumoxytol, a novel ultrasmall superparamagnetic iron oxide (USPIO)-based blood pool agent. *J. Magn. Reson. Imaging* 21, 46–52 (2005).

172 Artemov D. Molecular magnetic resonance imaging with targeted contrast agents. *J. Cell. Biochem.* 90, 518–524 (2003).

173 Artemov D, Bhujwalla ZM, Bulte JW. Magnetic resonance imaging of cell surface receptors using targeted contrast agents. *Curr. Pharm. Biotechnol.* 5, 485–494 (2004).

174 Bulte JW, Zhang S, van Gelderen P *et al.* Neurotransplantation of magnetically labeled oligodendrocyte progenitors: magnetic resonance tracking of cell migration and myelination. *Proc. Natl Acad. Sci. USA* 96, 15256–15261 (1999).

175 Remsen LG, McCormick CI, Roman-Goldstein S *et al.* MR of carcinoma-specific monoclonal antibody conjugated to monocrystalline iron oxide nanoparticles. the potential for noninvasive diagnosis. *Am. J. Neuroradiol.* 17, 411–418 (1996).

176 Weissleder R, Moore A, Mahmood U *et al.* *In vivo* magnetic resonance imaging of transgene expression. *Nat. Med.* 6, 351–355 (2000).

177 Moore A, Weissleder R, Bogdanov A. Uptake of dextran-coated monocrystalline iron oxides in tumor cells and macrophages. *J. Magn. Reson. Imaging* 7, 1140–1145 (1997).

178 Fleige G, Seeberger F, Laux D *et al. In vitro* characterization of two different ultrasmall iron oxide particles for magnetic resonance cell tracking. *Invest. Radiol.* 37, 482–488 (2002).

179 Stroh A, Zimmer C, Gutzeit C *et al.* Iron oxide particles for molecular magnetic resonance imaging cause transient oxidative stress in rat macrophages. *Free Radic. Biol. Med.* 36, 976–984 (2004).

180 Schnorr J, Wagner S, Abramjuk C *et al.* Comparison of the iron oxide-based blood-pool contrast medium VSOP-C184 with gadopentetate dimeglumine for first-pass magnetic resonance angiography of the aorta and renal arteries in pigs. *Invest. Radiol.* 39, 546–553 (2004).

181 Schnorr J, Wagner S, Abramjuk C *et al.* Focal liver lesions. SPIO-, gadolinium-, and ferucarbotran-enhanced dynamic T1-weighted and delayed T2-weighted MR imaging in rabbits. *Radiology* 240, 90–100 (2006).

182 Taupitz M, Schnorr J, Pilgrimm H, Hamm B, Wagner S. CMR 2005: 2.03: VSOP-C184 as contrast agent for MRI of atherosclerotic plaques: experimental results in rabbits. *Contrast Media Mol. Imaging* 1, 55 (2006).

183 Achiam MP, Løgager VB, Chabanova E, Eegholm B, Thomsen HS, Rosenberg J. Diagnostic accuracy of MR colonography with fecal tagging. *Abdom. Imaging* 34(4), 483–490 (2009).

184 Petrillo A, Catalano O, Delrio P *et al.* Post-treatment fistulas in patients with rectal cancer. MRI with rectal superparamagnetic contrast agent. *Abdom. Imaging* 32(3), 328–331 (2007).

185 Blomqvist L, Ohlsén H, Hindmarsh T, Jonsson E, Holm T. Local recurrence of rectal cancer: MR imaging before and after oral superparamagnetic particles vs contrast-enhanced computed tomography. *Eur. Radiol.* 10(9), 1383–1389 (2000).

186 Frank JA, Miller BR, Arbab AS *et al.* Clinically applicable labeling of mammalian and stem cells by combining superparamagnetic iron oxides and transfection agents. *Radiology* 228(2), 480–487 (2003).

187 Mohapatra S, Pramanik P. Synthesis and stability of functionalized iron oxide nanoparticles using organophosphorus coupling agents. *Colloids Surfaces A: Physicochem. Eng. Aspects* 339(1–3), 35–42 (2009).

188 Zhang C, Wängler B, Morgenstern B *et al.* Silica- and alkoxysilane-coated ultrasmall superparamagnetic iron oxide particles. a promising tool to label cells for magnetic resonance imaging. *Langmuir* 23(3), 1427–1434 (2007).

189 Cho S-J, Jarrett BR, Louie AY, Kauzlarich SM. Gold-coated iron nanoparticles: a novel magnetic resonance agent for *T*1 and *T*2 weighted imaging. *Nanotechnology 17*, 640–644 (2006).

## ■ Patent

201 Gruell H, Boeve H, Markov D. Clustered magnetic particles as tracers for magnetic particles imaging.
Patent no: WO/2009/027937

## ■ Website

301 National Cancer Institute definition of ferumoxytol
www.cancer.gov/Templates/drugdictionary.aspx?CdrID=377345